TECH LIBRARY KAFB, NM
0061176

NASA CONTRACTOR REPORT

NASA CR-2
c.1

NASA CR-2090

LOAN COPY: RETURN TO
AFWL (DOUL)
KIRTLAND AFB, N. M.

VORTEX EQUATIONS: SINGULARITIES, NUMERICAL SOLUTION, AND AXISYMMETRIC VORTEX BREAKDOWN

by Hartmut H. Bossel

Prepared by
UNIVERSITY OF CALIFORNIA
Santa Barbara, Calif. 93106
for Langley Research Center

NATIONAL AERONAUTICS AND SPACE ADMINISTRATION • WASHINGTON, D. C. • JULY 1972

TECH LIBRARY KAFB, NM

0061176

1. Report No.	2. Government Accession No.	3. Recipient's Catalog No.
NASA CR-2090		

4. Title and Subtitle	5. Report Date
VORTEX EQUATIONS: SINGULARITIES, NUMERICAL SOLUTION, AND AXISYMMETRIC VORTEX BREAKDOWN	July 1972
	6. Performing Organization Code

7. Author(s)	8. Performing Organization Report No.
Hartmut H. Bossel	

9. Performing Organization Name and Address	10. Work Unit No.
University of California Santa Barbara, California	126-13-10-01
	11. Contract or Grant No.
	NGR 05-010-025
	13. Type of Report and Period Covered
	Contractor Report

12. Sponsoring Agency Name and Address	14. Sponsoring Agency Code
National Aeronautics and Space Administration Washington, D. C. 20546	

15. Supplementary Notes

16. Abstract

A method of weighted residuals for the computation of rotationally symmetric quasi-cylindrical viscous incompressible vortex flow is presented and used to compute a wide variety of vortex flows. The method approximates the axial velocity and circulation profiles by series of exponentials having $(N + 1)$ and N free parameters, respectively. Formal integration results in a set of $(2N + 1)$ ordinary differential equations for the free parameters. The governing equations are shown to have an infinite number of discrete singularities corresponding to critical values of the swirl parameter. The computations point to the controlling influence of the inner core flow on vortex behavior. They also confirm the existence of two particular critical swirl parameter values: one separates vortex flow which decays smoothly from vortex flow which eventually breaks down, and the second is the first singularity of the quasi-cylindrical system, at which point physical vortex breakdown is thought to occur.

17. Key Words (Suggested by Author(s))	18. Distribution Statement
Vortex Equations Axisymmetric Vortex Breakdown Numerical Solution of Vortex Breakdown Tip and Leading-Edge Vortices	Unclassified - Unlimited

19. Security Classif. (of this report)	20. Security Classif. (of this page)	21. No. of Pages	22. Price*
Unclassified	Unclassified	74	$3.00

*For sale by the National Technical Information Service, Springfield, Virginia 22151

VORTEX EQUATIONS: SINGULARITIES, NUMERICAL SOLUTION, AND AXISYMMETRIC VORTEX BREAKDOWN

Hartmut H. Bossel
Mechanical Engineering Department
University of California
Santa Barbara, California

SUMMARY

A viscous parabolic subset of the incompressible Navier-Stokes equations, the quasi-cylindrical vortex equations, can be used to compute vortex flows as long as their stream surface angle remains small. At low values of a swirl parameter, computation presents no difficulties. At high swirl values, singularities are encountered which indicate a failure of the quasi-cylindrical approximation and are thought to be associated with physical axisymmetric vortex breakdown. 'Vortex breakdown' is normally followed by a 'vortex bubble', and a 'vortex jump' may occur farther downstream.

It is found that the quasi-cylindrical vortex equations have an infinite number of discrete swirl-dependent singularities whose corresponding critical swirl values depend on velocity and circulation profile shapes. The behavior of flow (deceleration vs. acceleration on the vortex axis) is opposite on both sides of a singularity (i.e. at higher or lower swirl). At high swirls, the approach to singularities can only be avoided by application of specific external axial velocity and/or circulation gradients. The singularities appear to correspond to the critical swirl values of the equation of inviscid rotating flow.

The first singularity S_1 is of particular significance as it seems to correspond to the often observed axisymmetric explosive breakdown. The physical significance of the higher

singularities is not quite clear at present. A second important value of the swirl parameter is S_o which separates flow which decays smoothly from vortex flow which eventually breaks down.

Typical vortex flows (initially uniform axial flow, leading edge vortex, trailing vortex) are computed for a wide variety of initial swirl parameters using a method of weighted residuals which expresses the velocity and circulation approximations in terms of exponentials. The effects of external axial velocity and circulation gradients are investigated.

TABLE OF CONTENTS

LIST OF SYMBOLS

a_n	parameter in the velocity approximation	[-]
b_n	parameter in the circulation approximation	[-]
$A_{n,k}$, $B_{n,k}$, C_k, D_k, E_k, F_k, $\bar{A}_{n,k}$, $\bar{B}_{n,k}$, $\bar{C}_k$, $\bar{D}_k$, $\bar{E}_k$, $\bar{F}_k$	coefficients in the ordinary differential equations (defined in the Appendix)	[-]
e	= 2.71828183	[-]
$f_k(Y)$	weighting functions	[-]
$g_k(Y)$	weighting functions	[-]
H	= VR (nondimensional parameter)	[-]
j_{1n}	zeros of the Bessel function J_1	[-]
k	= wr circulation	$[L^2/T]$
K	= WR nondimensional circulation	[-]
K_e	nondimensional external circulation	[-]
K_{e_i}	initial K_e	[-]
N	number of parameters in the velocity and circulation approximations	[-]

p	pressure	$[F/L^2]$
p_e	external static pressure	$[F/L^2]$
p_o	free-stream total pressure	$[F/L^2]$
P	$= p/\rho u_\infty^2/2)$ nondimensional pressure	[-]
P_e	nondimensional external static pressure	[-]
P_o	nondimensional free-stream total pressure	[-]
P_∞	nondimensional free-stream static pressure	[-]
r	radial coordinate	[L]
r_c	vortex core radius	[L]
R	$= \sqrt{Re}\ r/r_c$ nondimensional radial coordinate	[-]
R_c	nondimensional vortex core radius	[-]
Re	$= u_\infty r_c/\nu$ - core Reynolds number	[-]
S	swirl parameter $S = w_c/u_{ax} = W_c/U_{ax}$ or $S = (dW/dR)_{ax} R_c/U_{ax}$	[-]
$S(X)$	x-dependent swirl parameter as function of velocity profile development	[-]
S_{c_r}	values of S at which singularities exist	[-]
S_i	initial swirl parameter	
S_o	critical swirl parameter value (velocity profile-dependent) separating vortex flow which decays smoothly ($S<S_o$) from vortex flow which eventually "breaks down" ($S_o<S<S_1$)	[-]
$S_1, S_2,$	. . . singular swirl values (velocity profile-dependent) where singularities of quasi-cylindrical vortex equations occur	[-]
u	axial velocity (x-direction)	[L/T]
u_e	external axial velocities	[L/T]
u_∞	free-stream axial velocity	[L/T]
U	$= u/u_\infty$ nondimensional axial velocity	[-]
U_e	nondimensional external axial velocity	[-]
U_{e_i}	initial U_e	[-]
v	radial velocity (r-direction)	[L/T]

v_e	external radial velocity	[L/T]
V	$= \sqrt{Re}\ (v/u_\infty)$ nondimensional radial velocity	[-]
w	swirl velocity (circumferential direction)	[L/T]
w_c	swirl velocity at core radius r_c	[L/T]
W	$= w/u_\infty$ nondimensional swirl velocity	[-]
W_c	$= w_c/u_\infty$	[-]
x	axial coordinate	[L]
X	$= x/r_c$ nondimensional axial coordinate	[-]
X_f	nondimensional position of computational failure	[-]
X_o	x value at which velocity gradient is applied	[-]
Y	$= R^2/2$ nondimensional radial coordinate	[-]
α	exponent in velocity and circulation approximations	[-]
γ	exponent in the circulation profile	[-]
η	$= e^{-\alpha Y}$	
ν	kinematic viscosity	$[L^2/T]$
ρ	density	$[M/L^3]$
σ_k	weighting function exponent	[-]
$\phi(Y)$	complete set of linearly independent functions	[-]
.	d/dx	
'	d/dY	[-]

Subscripts:

k	integer, $1 \leq k \leq N + 1$
n	integer, $1 \leq n \leq N$
ax	on the axis

I. INTRODUCTION

1.1 Physics of the Problem

The present report presents and discusses numerical solutions to a specific parabolic subset - applicable to quasi-cylindrical vortex flows - of the axisymmetric incompressible Navier-Stokes equations. This subset can be used as a reasonable approximation for many vortex flows occurring in technological applications and in nature (wing vortices, rotating tubes, swirling pipe flow, dust devils, tornados). Solutions of the quasi-cylindrical vortex equations are therefore of some interest in their own right, but of even greater interest are perhaps the conditions under which solutions cannot be obtained. In such cases the physics of the problem are different than assumed in the quasi-cylindrical approximation, and this subset becomes inadequate. When this happens, the physical counterpart of the flow under consideration most likely experiences a rapid expansion or contraction of the core to violate the condition of quasi-cylindricity.

Observations of vortex flows at high swirl do indeed show rapid expansions and/or contractions under certain conditions. The observed closely-related phenomena have been lumped under the headings of 'vortex breakdown' and 'vortex bursting', and several explanations have been advanced. Until recently a peculiarity of vortex flows - their extreme sensitivity to probe insertion - has prevented the gathering of reliable experimental data to verify these explanations. Only now, with the advent of probeless velocity measurement using the laser Doppler anemometer, can reliable data be collected, and theories be checked and assigned their proper place in the overall flow picture. It turns out - once more - that the conflicting theories are not really in conflict after all, but that they describe different phenomena which are indeed observed to often happen more or less under the same circumstances.

In order to put the results of this study into the proper physical perspective, an interpretation of 'vortex breakdown' observations will first be made partly based on recent laser anemometer studies which have lead to some unexpected observations. The conclusions contrast some interpretations still to be found in the current literature.

Earlier experimental and theoretical work in the area of concentrated vortex flows has been reviewed in Hall (1966a), and a very comprehensive bibliography to 1967 is given in Timm (1967). A review of vortex breakdown has recently been made by Hall (1972), and a comprehensive review of confined vortex flows is due to Lewellen (1971). Observations of wing vortex flows and vortex breakdown, especially on delta wings, are numerous - references can be found in the reviews cited. With very few exceptions (especially Hummel 1965, McCormick et al. 1968) these studies are qualitative. It is expected that reliable quantitative data for wing vortex flows will become available in the near future with the advent of two- and three-dimensional and rapid scanning laser Doppler anemometers.

Much useful information on the phenomenon of vortex breakdown has come from the study of swirling flow in pipes (in particular Harvey 1962, Sarpkaya 1971a, 1971b, Orloff 1971, Orloff and Bossel 1971). The dye studies of Harvey and Sarpkaya are qualitative only, and the conclusions of these authors have been somewhat revised by the quantitative optical velocity measurements of Orloff and Bossel. More information on the vortex breakdown phenomenon has come from the study of flow in a stationary cylinder with a rotating lid (Maxworthy 1967, Vogel 1968). In the careful and comprehensive work of Vogel quantitative data on vortex breakdown are obtained from tracer studies. Swirling flows undergoing a rapid expansion have been studied by Gore and Ranz (1964), Nissan and Bresan (1961), Potter et al. (1958), So (1967), Vonnegut (1954) and others.

Several conflicting explanations have been advanced to explain the sudden expansion of vortex cores, most commonly referred to as 'vortex breakdown': the spiral instability theory of Ludwieg (1962, 1965), the hydraulic jump analogy of Benjamin (1962), or, in a milder form, the concept of a stationary wave (Benjamin 1967, Leibovich 1968), and finally the explanation on the basis of stationary continuous solutions of the Navier-Stokes equations for swirling flow, or a proper subset thereof (Vaisey 1956, Lavan and Fejer 1966, Bossel 1967, 1969, Orloff 1971, Orloff and Bossel 1971, Torrance and Kopecky 1971). On the other hand, the failure of the quasi-cylindrical subset of the Navier-Stokes equations (i.e. the failure of the quasi-cylindrical approximation in regions of rapidly expanding or contracting vortex flow) has been used by Gartshore (1963), Hall (1966b), Bossel (1967, 1971), Mager (1971) to predict the position of likely breakdown and the behavior of flow preceding it.

Most experimental observations seem to support the view that the sudden expansion of vortex cores is most often an axisymmetric phenomenon and not the result of spiral instability. However, according to unpublished experiments (Ludwieg 1971, private communication), spiral instability may indeed play a major role in the breakdown of delta wing vortices. Other instabilities have been identified by Sarpkaya (1971a,b), but the dominant role in what we know as the 'breakdown'-process appears to be a sudden axisymmetric expansion of the core. It is for this reason that the axisymmetric equations are studied in the present work. Before entering into the analysis, it will be useful to piece together a comprehensive picture of the axisymmetric 'vortex breakdown'-process based on the most recent quantitative data obtained through optical velocity measurements by Orloff (1971) and Orloff and Bossel (1971). It is found that the explanations and theories proposed so far all have their proper place and are not really competitive. The proper range of application will be identified.

Consider first a vortex flow with more or less cylindrical external stream surfaces and a high 'swirl' (some ratio of a representative circumferential (swirl) velocity to a representative axial velocity). An adverse pressure gradient is superimposed on the axis by the presence of an axisymmetric obstacle (Orloff and Bossel 1971). The flow observed is then as shown in Fig. 1.1. The flow initially approaches the obstacle in a quasi-cylindrical manner. The velocity on the axis decreases until a stagnation point is reached on the axis and flow has to move outward from the axis near the stagnation point. In keeping with traditional notation, this particular process will be called 'vortex breakdown' in the following.

There is reversed (upstream) axial flow on the downstream side of the stagnation point. This reversed flow is part of the flow in the ('forced') 'vortex bubble' between stagnation point and obstacle, a closed region with practically no interchange of fluid with the surrounding flow. The external flow passes over the bubble and over the rear of the obstacle. As it passes over the rear it undergoes a 'vortex jump' in the sense of the hydraulic jump analogy of Benjamin (1962), with a substantial loss of axial momentum and an attendant expansion of stream surfaces near the axis.

In Fig. 1.2 the stagnation point, and the rapid expansion near the axis are caused by the effect of an external pressure gradient such as produced by a flow divergence. With a proper favorable pressure gradient the bubble will contract downstream and may even be more or less closed. Flows having such (seemingly) closed 'free' vortex bubbles can either be generated by proper shaping of an outer surface as in Fig. 1.2 (Bossel and Orloff 1971, unpublished) or by a self-induced process between vortex bubble and external flowfield as in the vortex tube flows of Harvey (1962) and Sarpkaya (1971a,b). Sarpkaya has even succeeded in generating several vortex bubbles in a row. Just downstream of a vortex bubble a vortex jump may

occur, but does not appear to occur in many cases where the bubble is smooth or repeated. Following Benjamin (1967) and Leibovich (1968) these vortex bubbles can be viewed as solitary waves. However, their description appears to be more straightforward and accessible to numerical quantitative analysis if direct use is made of the Navier-Stokes equations or a proper subset of these equations.

Fig. 1.3 shows another possibility which appears to be typical of delta wing vortex flows and some tornados. In this case the vortex bubble following the vortex breakdown is not closed downstream. At some distance from the breakdown point the flow again becomes more or less cylindrical. In other flows (on delta wings, for example) a stagnation point occasionally does not seem to exist; there is only a swelling of the core with an attendant decrease of velocities in the core. This situation is depicted in Fig. 1.4; the term 'vortex bursting' should probably be reserved for it.

Finally, if the swirl is very high in a vortex, the vortex assumes a decidedly different columnar character where flow dependence on axial position has essentially disappeared, and the 'Taylor column' stretches far downstream (Fig. 1.5). This structure is found downstream of a vortex jump or immediately downstream of the flow entrance if the initial swirl is very high. In keeping with accepted notation (Benjamin 1962) this flow is termed 'subcritical' while the flow upstream of a vortex jump would be 'supercritical'. (Stationary waves may occur in 'subcritical' flow, while in 'supercritical' flow the axial flow is too fast, sweeping any waves downstream).

Summarizing the experimental observations, it is obvious that clear distinctions exist between 'vortex breakdown' and 'vortex jump', 'supercritical' and 'subcritical' flow, 'vortex breakdown' and 'vortex burst','axisymmetric breakdown' and nonaxisymmetric instabilities. For convenience, we have also

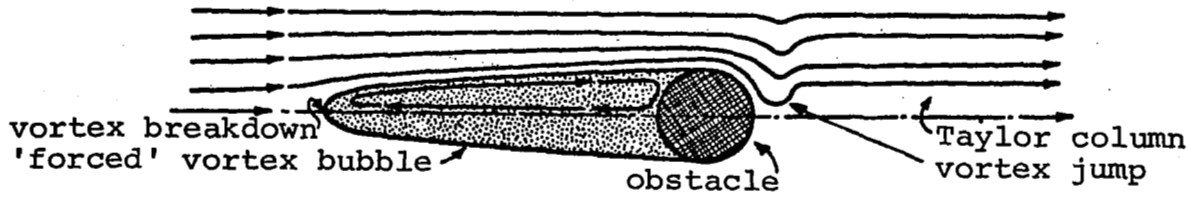

Fig. 1.1 Vortex breakdown caused by presence of an obstacle on the axis.

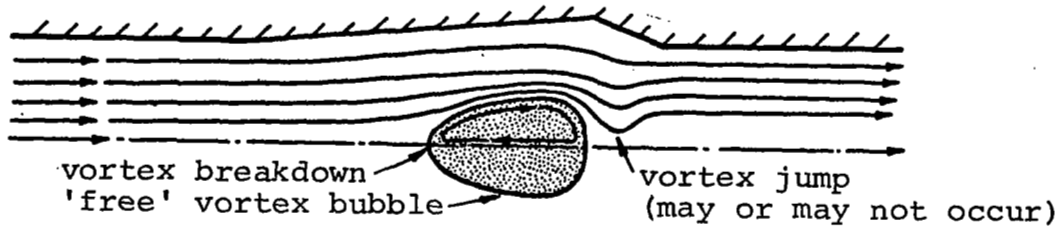

Fig. 1.2 'Free' vortex breakdown with 'closed' bubble.

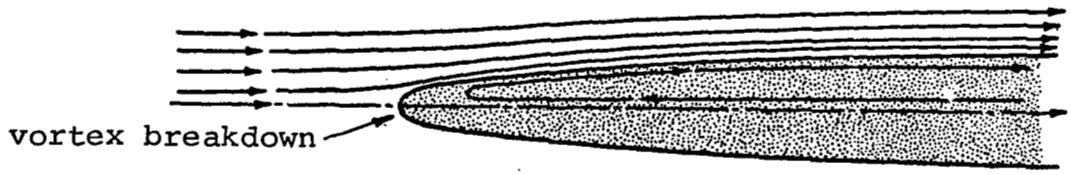

Fig. 1.3 'Free' vortex breakdown with 'open' bubble.

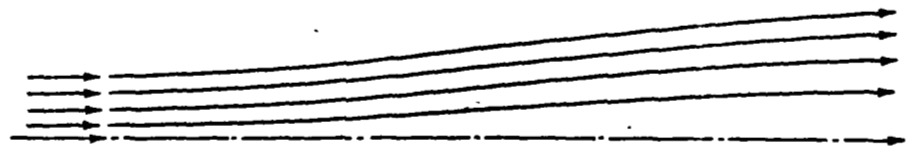

Fig. 1.4 Expansion of vortex core; no breakdown with free stagnation point.

Fig. 1.5 Subcritical (Taylor column) behavior.

distinguished between 'free' and 'forced' vortex bubbles, although they appear to be the result of the same basic mechanism. In this report, the term 'vortex breakdown' will be used to designate conditions where the quasi-cylindrical solutions become singular and the corresponding computations fail. This includes rapid core expansion, as in the vicinity of the first stagnation point, and rapid core contraction.

With accurate optical velocity measurements ahead of, around, behind, and in the vortex bubble now available (Orloff 1971, Orloff and Bossel 1971), it has become possible to test the accuracy and applicability of numerical approaches to the solution of the 'vortex breakdown' problem. It is found that the quasi-cylindrical approximation can be correctly applied upstream to a distance of the order of the bubble diameter ahead of the stagnation point (Figs. 1.1-1.3). Flow in the neighborhood of the stagnation point and in and around the bubble must be treated by using either the full Navier-Stokes equations or a proper approximate subset (Figs. 1.1-1.3). It was shown in Bossel (1967) that the proper subset is the equation for inviscid rotating flow. Numerical solutions show excellent quantitative agreement with the measured velocity profiles with an inaccurate description of the swirl velocity profile inside the bubble as the only exception (Orloff and Bossel 1971). For accurate description of the very slow flow inside the bubble, viscous terms should be taken into account; however the exact bubble shape and the external flow are quite obviously determined almost solely by the inviscid flowfield. The inviscid equation of rotating flow can be applied to compute 'free' and 'forced' vortex bubbles equally well (Bossel 1967, 1969, Orloff 1971, Orloff and Bossel 1971).

A continuous solution is not possible in a region where a vortex jump occurs; the 'flow force' concepts of Benjamin (1962) must then be applied to join two conjugate flows. In the

observations of Orloff and Bossel (1971) the vortex jump occurs over a distance of approximately one bubble diameter and is marked by very strong turbulence.

1.2 Swirl Parameter

The axisymmetric behavior of a vortex flow is very much a function of its swirl. A swirl parameter can be defined as the ratio of some representative (circumferential) swirl velocity to a representative axial velocity (see Sec. III). For zero swirl, the flow reduces to a jet or wake, depending on whether a velocity excess or deficit exists on the axis. This jet or wake velocity profile will ultimately decay to the freestream velocity as the flow proceeds downstream. The same is true for small and medium amounts of swirl, until the swirl velocity and axial velocity reach comparable magnitudes. At higher swirl parameters, the asymptotic approach to freestream conditions is replaced by deceleration of the flow on the axis until a stagnation point and subsequent 'breakdown bubble', or at least a swelling of the core appear. All other conditions being equal, there is obviously one particular swirl parameter value which divides a vortex flow which decays in a wake-like manner from another which 'breaks down'. This dividing swirl parameter is designated S_o in the following; it is a function of the vortex velocity profiles.

Axisymmetric vortex breakdown is a completely symmetric phenomenon with its origin at the very axis (Sarpkaya 1971a,b, Orloff 1971). Thus conditions on the axis must be of vital importance in its inception. In particular, viscosity establishes rigid rotation at and near the axis. For a rigidly rotating inviscid cylindrical slug of fluid of radius r_c, axial velocity u_{ax}, and swirl velocity w_c at r_c, a swirl parameter can be defined by $S = w_c/u_{ax}$, and two important theoretical results follow:

(1) As the swirl is increased and crosses $S_o = \sqrt{2}$ from below, an initial deceleration of the core element will amplify and lead to stagnation (Bossel 1968).

(2) As the swirl is increased further and crosses $S_1 = j_{11}/2$ (= 3.8317/2 = 1.9159)* from below, the character of the solution changes from 'supercritical' (which cannot support standing waves) to 'subcritical' (which can support standing waves) (Fraenkel 1956). As S reaches the values $j_{1n}/2$ corresponding to higher zeros of the Bessel function J_1, more waves appear.

It can be expected that the critical swirl values S_o, S_1, S_2, . . . of a viscous vortex will be a function of the vortex velocity profiles and will be somewhat different from those for the rigidly rotating inviscid cylindrical slug. Of particular significance for vortex flows are S_o (dividing wake-type from breakdown behavior) and S_1 (beyond S_1 substantial upstream influence is possible).

1.3 Numerical Approach

Laminar incompressible steady axisymmetric vortex flows are described by the corresponding form of the Navier-Stokes equations. These equations can be approximated by a parabolic viscous set, analogous to the boundary layer equations, in regions where the stream surface angle remains small (quasi-cylindrical vortex flow), and by the inviscid equations of rotating flow at and near the axis, and where stream surface angles become large (expansion or contraction of the core) (Bossel 1969).

Some solutions of the inviscid set pertaining to vortex flows at high swirl have been presented in Bossel (1967, 1969), Chow (1969), Orloff and Bossel (1971); here we shall now discuss

* j_{11} is the first zero of the Bessel function J_1.

a method of solving the parabolic viscous set and give corresponding results for different swirl parameters, initial velocity profiles, and external pressure and circulation gradients. Since the regions of validity of the two sets partially overlap on and near the axis, it should be possible to confirm some of the earlier results. The parabolic system has been used before in numerical computations by different methods (Gartshore 1963, Hall 1965, Bossel 1967, Mager 1971). Gartshore and Mager each used a momentum-integral approach and encountered a singularity which they linked to the vortex breakdown phenomenon and to the critical swirl parameter 3.8317/2 of flow in initially rigid rotation. The present results reinforce this view. Beyond this critical swirl ratio, Bossel (1967) and Mager (1971) also obtained flows which contrasted in behavior with those below the critical swirl ratio.

The numerical method (N-parameter 'exponential series integral method'*) to be used for the present study has previously been outlined in Bossel (1970a, 1971). A related method (N-parameter 'power series integral method') has earlier been used successfully to calculate viscous vortex flows (Bossel 1967). The methods were inspired by the success of the Dorodnitsyn method for the calculation of boundary layers (Dorodnitsyn 1962, Bethel 1968), especially by its aspects of speed and accuracy. However, the Dorodnitsyn approach with its use of Y(U) in place of U(Y) cannot be directly applied to vortex flows where axial velocity profiles often exhibit overshoot and flow reversal. The present approach circumvents this problem. The soundness of the exponential series integral method has been demonstrated in its application to incompressible and compressible boundary layer flows (Bossel 1970a,b, Mitra and Bossel 1971).

---

* The term 'integral method' is used here to avoid the cumbersome (but more accurate) terms 'method of weighted residuals' or 'method of integral relations'.

There are good reasons for choosing an N-parameter integral method over a finite difference method for a study such as the present one. Many of the open questions in this case only require a qualitative answer, which can be obtained at minimal computing cost by a one or two parameter solution. If accuracy is desired, the number of parameters is increased without any change in the program. Results of the same detail and accuracy as for finite difference methods can then be obtained. The integral approach reduces the solution of partial differential equations to solution of a set of ordinary differential equations. Well-known stable integration schemes, such as the Runge-Kutta method, can be applied. There is little chance of confusing a true singularity of the set of equations to be solved with a singularity of a finite difference scheme replacing it. No iterations are necessary. Finally, velocities, stream function, pressure, boundary layer thickness, shear, etc., can all be computed simply and directly from analytical expressions involving the parameters in the velocity approximations.

1.4 Overview

The following Section II will first describe the computational method and give an example for its accuracy and convergence. Singularities of the equations are investigated in Section III, and a swirl parameter is introduced. Section IV investigates, for constant external axial velocity and circulation, three vortex flows which are of particular interest to the fluid dynamicist: (1) vortex flow with initial uniform axial velocity, (2) vortex flow where the velocity on the axis is initially higher than the freestream velocity (leading edge vortex), and (3) vortex flow where the velocity on the axis is initially lower than the freestream velocity (trailing vortex). Representative velocity profiles and velocity distributions on the axis as a function of distance are given. The effects of positive or negative gradients in the external velocity and

circulation distribution are studied in Section V. Some conclusions are drawn, and results are summarized in Section VI.

II. COMPUTATIONAL METHOD

In developing a method of weighted residuals for a problem in two coordinates, the dependent variables in the partial differential equations are replaced by approximating functions, multiplied by a set of weighting functions, and then formally integrated with respect to one coordinate. There remains a set of ordinary differential equations in the other coordinate for the parameters in the approximating expressions for the dependent variables. The major task in developing the integral method is the correct development of the coefficients in the set of ordinary differential equations - not a difficult task, but one requiring careful bookkeeping. The FORMAC* method has been used in a case of comparable complexity to relegate this task to the computer (Mitra 1970). The ordinary differential equations are solved for the parameters by any of a number of standard methods. Knowledge of the parameters at each step permits calculation of the dependent variables and of a number of related variables of interest.

2.1 Governing Equations

The independent and dependent variables are introduced in Fig. 2.1. The dimensional equations for incompressible viscous quasi-cylindrical vortex flow are (Bossel 1969):

$$\frac{\partial u}{\partial x} + \frac{\partial v}{\partial r} + \frac{v}{r} = 0$$

$$\frac{w^2}{r} = \frac{1}{\rho}\frac{\partial p}{\partial r}$$

$$u\frac{\partial u}{\partial x} + v\frac{\partial u}{\partial r} = -\frac{1}{\rho}\frac{\partial p}{\partial x} + \nu\left(\frac{\partial^2 u}{\partial r^2} + \frac{1}{r}\frac{\partial u}{\partial r}\right)$$

$$u\frac{\partial w}{\partial x} + v\frac{\partial w}{\partial r} + \frac{vw}{r} = \nu\left(\frac{\partial^2 w}{\partial r^2} + \frac{1}{r}\frac{\partial w}{\partial r} - \frac{w}{r^2}\right) \qquad (2.1)$$

---

* FORmula MAnipulation on Computer, a method developed by IBM for non-numerical manipulations. It uses PL-1 or FORTRAN.

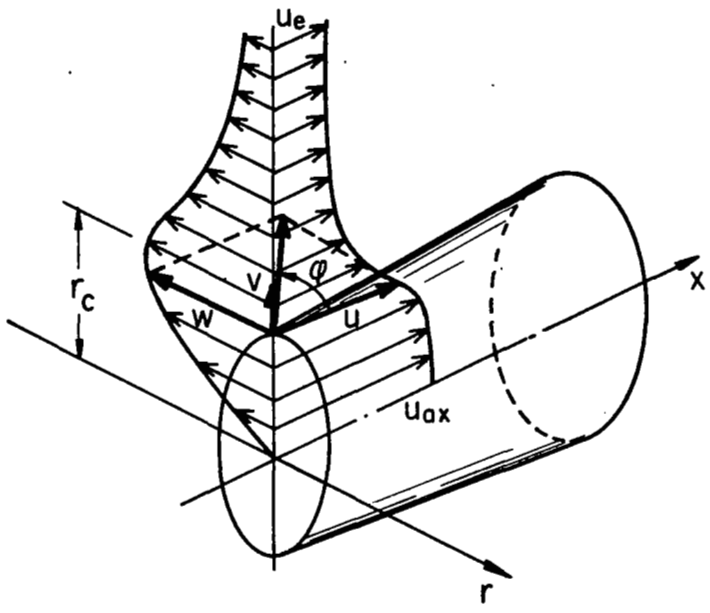

Fig. 2.1 Coordinate system and velocities.

with the boundary conditions:

at $r = 0$: $v = 0$, $w = 0$, $u = u_{ax}$ (free)

at $r \to \infty$: $u \to u_e(x)$, $wr = k \to k_e(x)$

Nondimensional variables are defined as follows:

$$X = x/r_c \qquad Y = R^2/2 = Re(r^2/2r_c^2) \qquad P = p/(\rho u_\infty^2/2)$$

$$U = u/u_\infty \qquad V = \sqrt{Re}\ (v/u_\infty) \qquad W = w/u_\infty$$

where the core Reynolds number $Re = u_\infty r_c/\nu$. For convenience we define $H = VR$ and $K = WR$ (circulation). These quantities are introduced into the conservation equations. The pressure P is eliminated by cross-differentiation, and two equations remain for U and K:

$$\frac{\partial}{\partial X}(UK) + \frac{\partial}{\partial Y}\left(HK - 2Y\frac{\partial K}{\partial Y} + 2K\right) = 0$$

$$\frac{\partial}{\partial X}\left(2Y^2U\frac{\partial U}{\partial Y} + \frac{K^2}{4}\right) + Y^2\frac{\partial^2}{\partial Y^2}\left(HU - 2Y\frac{\partial U}{\partial Y}\right) = 0 \qquad (2.2)$$

where

$$H = -\int_0^Y \frac{\partial U}{\partial X}\,dY$$

The boundary conditions now become:

at $Y = 0$: $H = 0$, $K = 0$, $U = U_{ax}$ (free)

at $Y \to \infty$: $U \to U_e(X)$, $WR = K \to K_e(X)$

The pressure at any point in the flow is given by

$$P = P_e - \int_Y^\infty \frac{K^2}{4Y^2}\,dY$$

where

$$P_e = P_o - U_e^2 = P_\infty + 1 - U_e^2$$

2.2 Integral Relations

As a first step in developing the computational method, integral relations are derived from the two momentum equations (2.2). In order to obtain a sufficient number of equations for determination of the unknown parameters in the axial velocity and circulation approximations to be introduced below, the equations are multiplied by members of two sets of weighting functions $g_k(Y)$ and $f_k(Y)$, respectively, and then integrated formally in the Y-direction from zero to infinity. To facilitate the integration, we require $g_k(0)$, $f_k(0)$ = finite, and $g_k(\infty)$, $f_k(\infty) = 0$. After integration by parts, rearrangement, and simplification:

$$\frac{d}{dX}\int_0^\infty g_k UK\,dY - \int_0^\infty g_k'HK\,dY - \int_0^\infty (2g_k''Y + 4g_k')K\,dY = 0$$

$$\frac{d}{dX}\int_0^\infty (f_k'Y^2 + 2f_kY)U^2\,dY - \frac{d}{dx}\int_0^\infty f_k\frac{K^2}{4}\,dY$$

$$-\int_0^\infty (f_K''Y^2 + 4Yf_k' + 2f_k)HU\,dY$$

$$-\int_0^\infty (2f_k'''Y^3 + 14f_k''Y^2 + 20f_k'Y + 4f_k)U\,dY = 0 \qquad (2.3)$$

2.3 Approximating and Weighting Functions

The integration is completed with the following choices for weighting functions and axial velocity and circulation approximations:

$$g_k(Y) = e^{-\sigma_k Y} \qquad k = 1, 2, \ldots, N$$

$$f_k(Y) = e^{-\sigma_k Y} \qquad k = 1, 2, \ldots, N+1$$

$$U(X,Y) = (1 - e^{-\alpha Y})\left[U_e(X) + \sum_{n=1}^{N} a_n(X)e^{-n\alpha Y}\right] + U_{ax}(X)e^{-\alpha Y}$$

$$K(X,Y) = W(X,Y)R = (1 - e^{-\alpha Y})\left[K_e(X) + \sum_{n=1}^{N} b_n(X)e^{-n\alpha Y}\right] \qquad (2.4)$$

The external velocity and circulation $U_e(X)$ and $K_e(X)$ are prescribed; the $a_n(X)$, $b_n(X)$ and the velocity on the axis $U_{ax}(X)$ are free parameters. Major reasons for these choices (Bossel 1970a) are the exponential character of the flows, ease of

analytical integration, the fact that the approximations satisfy the boundary conditions, and the observation that the approximations satisfy Weierstrass' approximation theorem after a coordinate transformation of the semi-infinite region $0 \leq Y < \infty$ into $1 \geq \eta > 0$, with $\eta = e^{-\alpha Y}$.

2.4 System of Ordinary Differential Equations

Introduction of the approximating expressions and the weighting functions (2.4) into equation (2.3) results in the following set of ordinary differential equations for U_{ax} and the parameters $a_n(X)$ and $b_n(X)$:

$$\sum_{n=1}^{N} \dot{a}_n A_{n,k} + \sum_{n=1}^{N} \dot{b}_n B_{n,k} + \dot{U}_{ax} C_k = -\dot{U}_e D_k - \dot{K}_e E_k - F_k$$

$$k = 1, 2, \ldots, N + 1$$

$$\sum_{n=1}^{N} \dot{a}_n \bar{A}_{n,k} + \sum_{n=1}^{N} \dot{b}_n \bar{B}_{n,k} + \dot{U}_{ax} \bar{C}_k = -\dot{U}_e \bar{D}_k - \dot{K}_e \bar{E}_k - \bar{F}_k$$

$$k = 1, 2, \ldots, N \qquad (2.5)$$

The coefficients are given in the Appendix. Only a small part of the coefficient calculation has to be done at each step; the major part is done only once at the beginning of the computation. The system (2.5) of (2N + 1) first order ordinary differential equations is first solved (by Gaussian elimination) for the derivative vector (da_n/dX; db_n/dX; dU_{ax}/dx). A standard method of integration then produces the a_n, b_n, and U_{ax} (the Runge-Kutta method has been used in the present work). Axial velocity $U(X,Y)$, circulation $K(X,Y)$, and swirl velocity $W(X,Y)$ follow from relations (2.4).

2.5 Initial Profiles

Initial profile parameters a_n, b_n, and U_{ax} for the initial axial velocity and circulation profiles (2.4) are required to start the calculation. In the present study, simple exponential profiles have been used throughout, i.e.,

$$U_{initial}(Y) = U_e(1 - e^{-\alpha Y}) + U_{ax}e^{-\alpha Y}$$

and

$$K_{initial}(Y) = K_e(1 - e^{-\alpha Y}) \text{ or } K_e(1 - e^{-2\alpha Y})$$

Exponents $\alpha = 1$, and $\sigma_k = k$, $k = 1, 2, \ldots, N + 1$ were used in all of the calculations.

In the case of arbitrary profiles, the parameters a_n, b_n, and U_{ax} are obtained as outlined in Bossel (1970a or b). The procedures for the axial velocity profile U(Y) and the circulation profile K(Y) are identical. Thus, if U(Y) is the (analytical or tabulated) profile to be approximated, $U_N(Y;a_n)$ the profile approximation (with unknown parameters a_n), and $f_k(Y)$ a convenient weighting function, then the N unknown parameters a_n are obtained from the N equations

$$\int_0^\infty f_k(Y)[U(Y) - U_N(Y;a_n)]\,dY = 0$$

$$k = 1, 2, \ldots, N$$

2.6 Accuracy and Convergence

Results of the present method were compared with previous computations (Bossel 1967) using polynomials in Y in the approximating functions. For N = 2 the agreement was within 3% in the velocity profiles. In cases where they can be compared, the computations appear to agree well with those of Hall (1966b) (only a qualitative comparison can be made, however, since Hall prescribes the outer stream surface shape). Critical runs have

been repeated with different orders N of approximation. Figures 2.2 and 2.3 show the velocity on the axis, swirl parameter, and profile development for a breakdown case (type 1b) and N = 1, 2, 3, 4, and 5. There is obvious convergence as N increases. Cases like these have typical running times on the IBM 360/75 of 5 to 15 seconds for N = 1 and 2, and 10 to 30 seconds for N = 3 to 5. All cases discussed later were run with N = 3, which appeared to be an efficient compromise between the conflicting demands of high accuracy and low computing time.

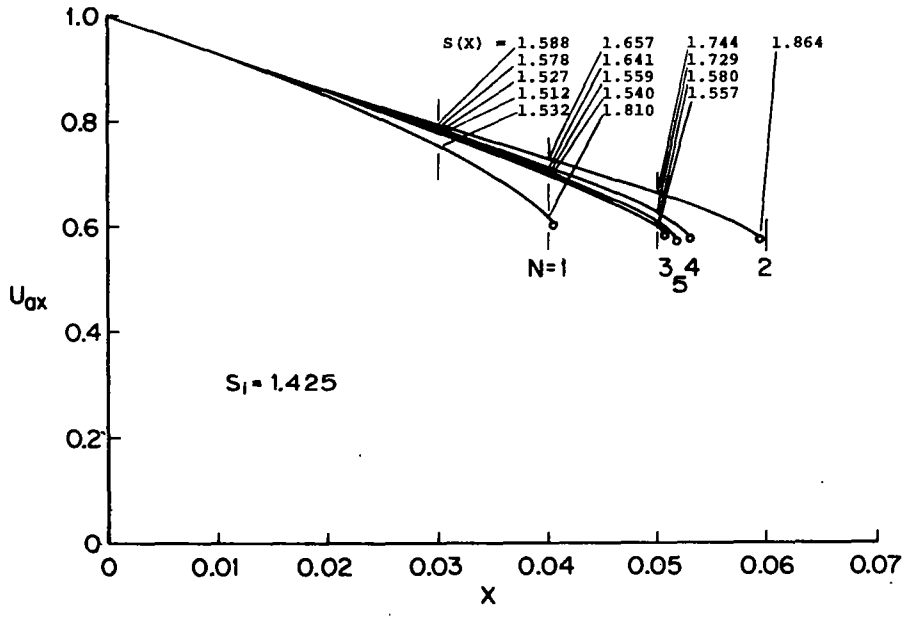

Fig. 2.2 Development of velocity on the axis and local swirl parameter S(X) as a function of number of parameters used, for initial swirl parameter S_i = 1.425.

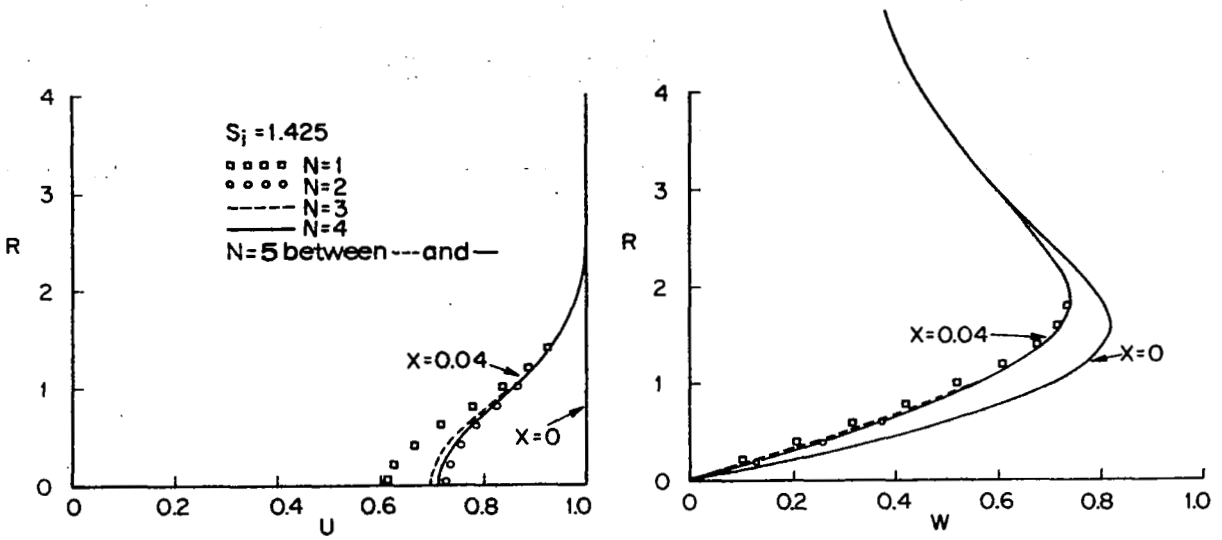

Fig. 2.3 Velocity profile development as a function of number of parameters used in the profile approximation.

III. SINGULARITIES AND CRITICAL SWIRL PARAMETERS

3.1 Singularities of the Governing System

The system of ordinary differential equations (2.5) becomes singular when the determinant of coefficients for the unknowns a_n, b_n, and U_{ax} vanishes, and the right-hand side remains nonzero. The special case when the right-hand side vanishes also has some significance and is considered later.

At a particular axial position X_o the profile shapes (relations 2.4) are determined by the local $a_n(X_o)$, $b_n(X_o)$, and $U_{ax}(X_o)$. Without loss in generality we shall assume $U_e = 1$ and keep only K_e as a free parameter. This amounts to investigating a given axial velocity profile and a given circulation profile shape at different values of external circulation K_e. The condition for vanishing of the determinant of coefficients on the left-hand side of system (2.5) is represented by a polynomial expression of the form

$$\sum_{n=0}^{N} G_n (K_e^2)^n = 0 \qquad (3.1)$$

with N roots for characteristic external circulation values (K_e^2). The G_n are numerical coefficients. Thus, there are N distinct values of K_e^2 which lead to singularities, and for $N \to \infty$ the following results obtain:

For a given axial velocity profile and given shape of the circulation profile, the equations of quasi-cylindrical viscous incompressible vortex flow (2.1) have a countably infinite set of singularities for discrete values of external circulation, $|K_e|$.

It should be stressed that the singularities are a function of the local profiles only and independent of local axial gradients of external axial velocity and circulation. However, the

profile development itself is, of course, dependent on external gradients.

The effect of gradients of external axial velocity U_e and circulation K_e (i.e. dU_e/dX and dK_e/dX) becomes obvious if the special case is considered where the right-hand side of equations (2.5) vanishes together with the determinant of coefficients . System (2.5) is then nonsingular. The right-hand side is a linear function of the gradients dU_e/dX and dK_e/dX and the parameters a_n, b_n, and U_{ax} in the axial velocity and circulation profiles. For each profile combination (i.e. U_e, K_e, a_n, b_n, U_{ax}) a particular combination of external axial and circulation gradients dU_e/dX and dK_e/dX exists for which the right-hand side vanishes and the system (2.5) is nonsingular, i.e.:

A singularity can be avoided by application of appropriate external axial and circulation gradients.

This result is supported by the results of computations for different external axial and circulation gradients described in this report.

The two results derived above are independent of the particular approximation and weighting functions chosen (i.e. expressions (2.4)) since any continuous function U(Y) or K(Y) can be represented by an infinite series of linearly independent functions $\{\phi_n(Y)\}$ forming a complete set.

It becomes evident from the analysis that the (swirl-dependent) singularities of the quasi-cylindrical vortex equations are different in character from the separation singularity of the boundary layer equations. In particular, in contrast to boundary layer solutions, there exist meaningful vortex solutions for swirl values between the singular values, and especially for a swirl value greater than that of the first singularity. Full vortex computations (Secs. IV and V) have shown, however, that these solutions will normally only persist for a finite distance, before they are driven to the next singularity.

3.2 Swirl Parameters

In comparing different vortex flows, K_e is not a very meaningful parameter. Since the axisymmetric breakdown behavior of vortex flows is evidently controlled by conditions at the very core (Sarpkaya 1971a,b, Orloff and Bossel 1971), a swirl parameter is introduced which is based on core conditions, i.e. the swirl velocity profile gradient on the axis, the axial velocity on the axis, and the core radius $R_{w\ max}$ where the swirl velocity W reaches its maximum value:

$$S = \frac{(dW/dR)_{ax}\ R_{w\ max}}{U_{ax}}$$

This definition of the swirl parameter reduces to the familiar one $S = \Omega R_c/U = W_c/U$ for a cylinder of fluid of radius R_c in rigid rotation Ω, with uniform axial velocity U. Inviscid solutions for such flows (Fraenkel 1956) have critical values of the swirl parameter at $j_{1n}/2$ = 1.9159, 3.5078, 5.0867, 6.6618, 8.2353, ..., where j_{1n} are zeros of the Bessel function J_1.

3.3 Singularities for Initially Uniform Axial Flow

Figure 3.1 presents the first five singularities for the vortex profiles

$$U(Y) = 1 = \text{constant}$$

$$K(Y) = WR = K_e(1 - e^{-\alpha Y}) = S(1 - e^{-\alpha Y})/0.792$$

as a function of swirl parameter and order of approximation used. This flow approximates rigid rotation in the core. The singularities were obtained by computing the derivatives $\dot{a}_n$, $\dot{b}_n$, $\dot{U}_{ax}$ over a wide range of K_e. Each additional approximating term accounts for a new singularity, as expected, while the location of previously computed singularities is only slightly affected.

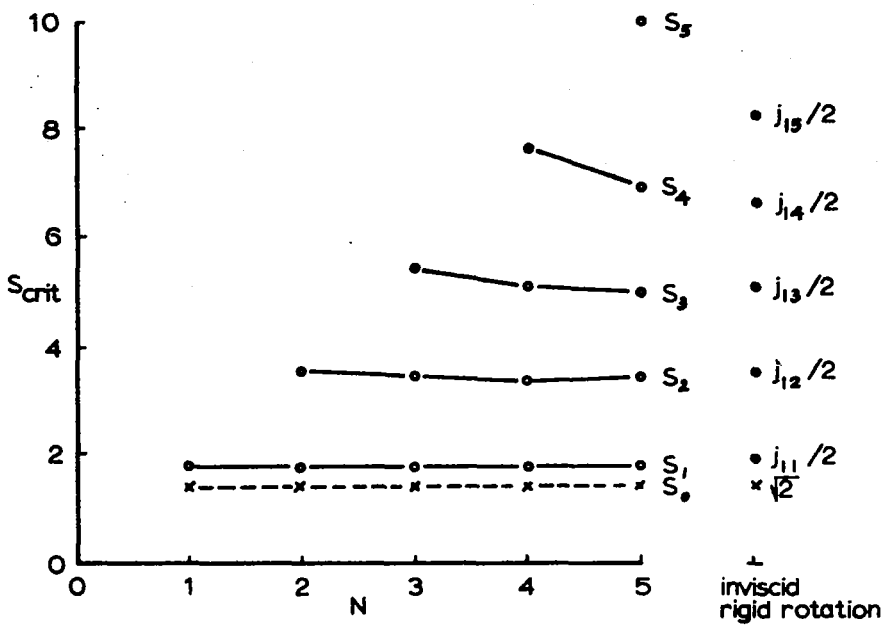

Fig. 3.1 Singular swirl parameter values for U(Y) = 1, and K(Y) = WR = $S(1-e^{-Y})/0.792$ as a function of order of approximation N. (Inviscid values are for rigid body rotation.)

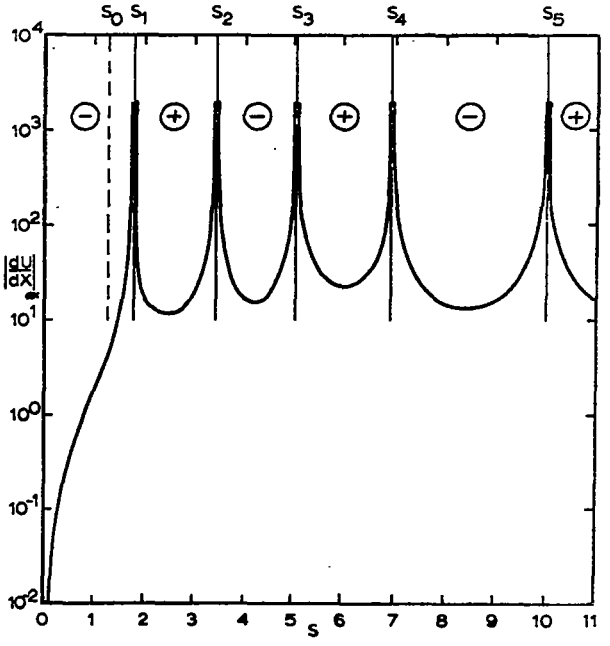

Fig. 3.2 Magnitude of gradient of velocity on the axis as function of swirl parameter. Uniform axial flow U(Y) = 1, and K(Y) = WR = $S(1-e^{-Y})/0.792$.

Likewise, the use of different α or weighting function exponents k has only minimal effect on the location of the lower order singularities. In particular, the singularity of greatest interest, S_1, remains practically constant. Since there is ample evidence that this first singularity is associated with axisymmetric vortex breakdown, computations failing at singularities, and in particular at S_1, will also be said to 'breakdown' in the following work. The critical swirl values $j_{1n}/2$ as found from the theory of inviscid rigid rotation (Fraenkel 1956) are also shown in Fig. 3.1. This figure also gives the swirl parameter S_o dividing flow which decays smoothly (type 1a) from flow which is abruptly decelerated on the axis and 'breaks down' because S_1 is reached (type 1b). The theoretical (inviscid) value (Bossel 1968) for uniform flow in initially rigid rotation is $S_o = \sqrt{2}$. The viscous value for S_o is found from a full vortex computation (see Sec. IV). There is striking agreement between the viscous and inviscid values for S_o, S_1, S_2, ...

3.4 Behavior of Axial Derivatives

At each singularity, all axial derivatives jump to infinity in magnitude and reverse signs. This results in contrasting behavior for flows separated by a singularity. The axial derivative of the velocity on the axis for the vortex with uniform axial flow is plotted in Fig. 3.2 as a function of swirl parameter S. The singularities are very evident. Note especially that the sign of the axial gradient reverses at each singularity. In particular, for a swirl value below S_1, the axial flow is decelerated in the core, while for a swirl value $S_1 < S < S_2$ the axial flow is accelerated in the inner core.

3.5 Effect of Velocity Profile

The critical swirl parameters S_o, S_1, S_2, ... are functions

of the a_n, b_n, U_{ax}, and U_e and are therefore profile-dependent. The example given, which approximates rigid rotation in its inner core, appears to confirm the earlier contention (Bossel 1967, 1968) that the behavior of viscous vortex flows is governed mainly by inviscid core properties. The effect of nonuniform initial axial flow on the critical swirl parameters is shown in Fig. 3.3 for the family of profiles

$$U(Y) = (1 - e^{-\alpha Y}) + U_{ax}e^{-Y} = 1 + e^{-\alpha Y}(U_{ax} - 1)$$

$$K(Y) = WR = K_e(1 - e^{-\alpha Y})$$

Flows with $U_{ax} < 1$ are of the trailing vortex type, with a velocity deficit on the axis, while flows with $U_{ax} > 1$ approximate the leading edge vortex with a velocity excess on the axis.

Figure 3.3 shows the same qualitative behavior for the various flows. The magnitudes of the critical swirl values for

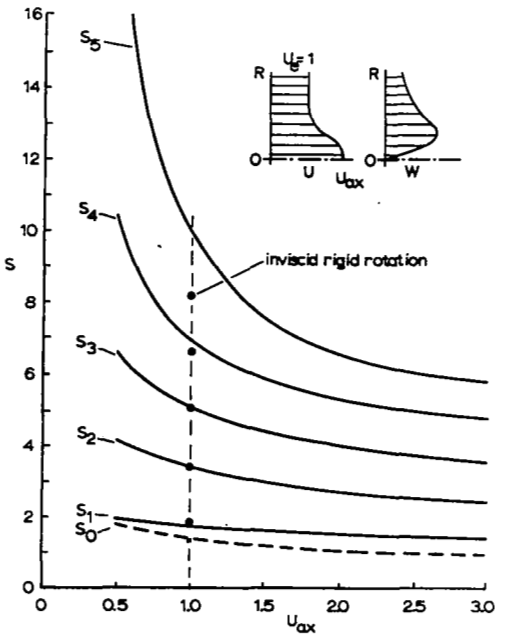

Fig. 3.3 Effect of velocity profile on the critical swirl values. $U(Y) = 1 + e^{-Y}(U_{ax}-1)$, $K(Y) = S(1-e^{-Y})/0.792$.

the nonuniform profiles show a profile effect: they are consistently higher for the profile with initial axial velocity deficit, and consistently lower for the profile with axial excess near the axis. This result is to be expected. The average velocity near the axis is most certainly higher than U_{ax} in the trailing vortex case due to the effect of faster flow in a neighborhood of the axis. In the case of the leading edge vortex, fluid surrounding the axis is slower than U_{ax} and the average velocity near the axis would be less. If proper average velocities were used in the calculation of S, the lines of critical swirl parameters would be more nearly horizontal.

Singularity analyses can be performed for any given arbitrary (experimental) axial and swirl velocity profile combination in order to obtain information on likely flow behavior, in particular the proximity of S_1. The coefficients a_n, b_n, and U_{ax} in an N-th order profile approximation (2.4) are first determined by the method of Bossel (1970a). The critical swirl values are then either obtained by determining the coefficients G_n in the characteristic equation (3.1) and solving for the first N critical K_e (or S_{cr}), or by determining the gradients $d/d\bar{X}$ of the a_n and b_n from system (2.5) as a function of K_e (or S).

3.6 Assessment of Breakdown Behavior

The results of this section offer several possibilities of assessing the probable axisymmetric breakdown behavior of vortex velocity profiles. In the order of increasing accuracy:

(1) Comparison of the swirl value

$$S = \frac{(dW/dR)_{ax} R_c}{U_{ax}} = \frac{(dw/dr)_{ax} r_c}{u_{ax}}$$

with the inviscid critical values for rigid rotation, in particular $S_o = \sqrt{2}$ (dividing stagnating ($S > S_o$) from

wake-type vortex flow ($S < S_o$)), and $S_1 = 1.9159$ (dividing supercritical ($S < S_1$) from subcritical vortex flow ($S > S_1$), with a reversal of behavior at S_1).

(2) Comparison of the computed swirl value with the results of Fig. 3.3.

(3) Approximation of the velocity profiles by parameters a_n, b_n, U_e, U_{ax}, K_e using the method in Bossel (1970a) for initial profile approximation. Using the approach of the present section, the axial gradients are then computed and the actual singularities determined by varying K_e or the swirl S.

IV. VORTEX COMPUTATIONS FOR CONSTANT EXTERNAL AXIAL VELOCITY AND CIRCULATION

This section presents results of vortex computations for constant external axial velocity and circulation. Three different initial velocity profiles were used in this and in the following section, corresponding to initially uniform axial flow and to flows of leading edge and trailing vortex type, respectively. Diagrams of distance X_f to failure of the computation as function of initial swirl parameter will first be presented for these three flow types. The development of the velocity on the axis and of the velocity profiles will be discussed in some detail. The results confirm the singular behavior predicted in Sec. III.

4.1 Initial Profiles and Distance to Failure

Uniform initial axial flow

The case where the initial axial velocity profile is uniform while the swirl velocity profile is linear with R in the vicinity of the axis provides a good test of the assertion that vortex behavior is governed by the inviscid properties of the rigidly rotating core as conditions on the axis are then identical in both cases. Initial profiles (Burgers 1940) for this case were

$$U(Y) = 1 = \text{constant}$$

$$K(Y) = W(Y)R = K_e(1 - e^{-\gamma Y})$$

Most computations presented here were obtained for $\gamma = 1$. $\gamma = 2$ was used to test scaling effects on the results of the computation. The differences were found to be minimal. The relationship between external circulation and initial swirl can be computed from the initial profiles. For $\gamma = 1$

$$S = \frac{(dW/dR)_{ax} R_c}{U_{ax}} = .792\ K_e/U_{ax} = .792\ K_e$$

and for $\gamma = 2$

$$S = 1.121\ K_e/U_{ax} = 1.121\ K_e$$

Figure 4.1 presents, as a function of initial swirl parameter and for N = 3, the distance of successful computation before failure occurred at X_f. This plot shows several distinct regions separated by singular points in accordance with the results of Sec. III. Continuous solutions could only be found in region 1a, corresponding to an initial swirl parameter $S \lesssim \sqrt{2}$. The characters of the solutions in the different regions will be discussed more fully in the next section. As pointed out in Sec. III, the computation with N = 3 only picks up the first three singularities. The results are therefore only accurate for $S \lesssim S_2$.

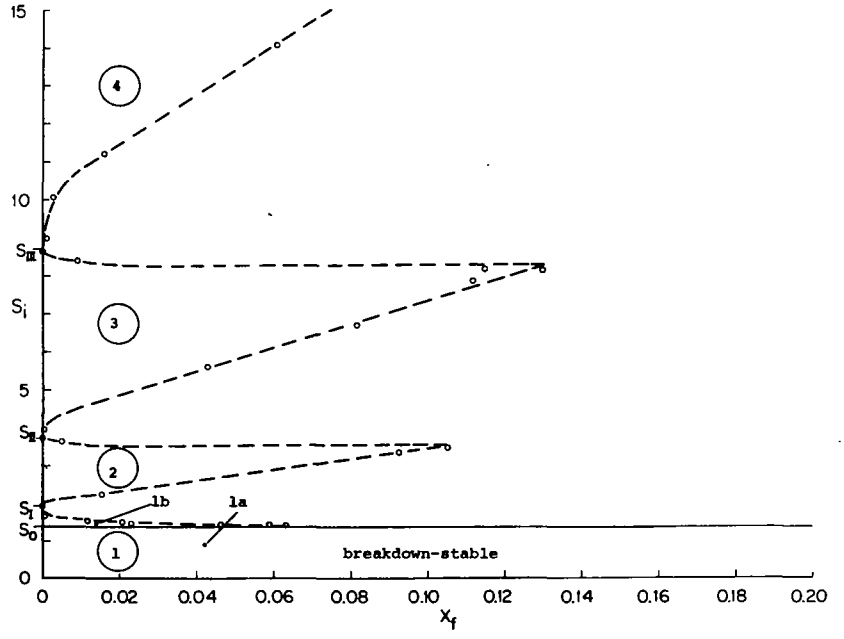

Fig. 4.1 Distance to failure (at X_f) as function of initial swirl parameter. Initially uniform axial flow. Open circles denote failure of computation.

Leading edge vortex

Experimental (Hummel 1965) and theoretical (Hall 1961) results for leading edge vortex flows (as generated at the leading edges of delta wings, for example) all show a large excess of axial velocity near the axis over the freestream axial velocity. It is of some interest to see what effect, if any, this velocity excess has on the vortex behavior. The effect of the nonuniform shape of the axial velocity profile on the critical swirl values has been discussed in Sec. III.

The initial velocity profiles investigated were

$$U(Y) = 1 + e^{-Y} \qquad \text{(i.e. } U_{ax} = 2.0,\ U_e = 1.0\text{)}$$

$$K(Y) = W(Y)R = K_e(1 - e^{-Y})$$

The relationship between K_e and S for these profiles is

$$S = .792\ K_e/U_{ax} = .792\ K_e/2 = .396\ K_e$$

This choice is not too good an approximation to the experimental and theoretical profiles of Hummel and Hall, but it should serve to demonstrate the effect of higher axial core velocity.

Distances to failure of the computation at X_f for N = 3 are shown in Fig. 4.2 as a function of initial swirl parameter. The behavior is qualitatively the same as for the case of initial uniform axial flow (Figure 4.1). The critical swirl values are now somewhat different from the previous case. They have been more accurately determined, with N = 5, in Sec. III.

Trailing vortex

The trailing vortex, as found downstream of a straight wing, has a wake-like axial velocity distribution with a core velocity smaller than the freestream velocity (Batchelor 1964, McCormick et al. 1968). This velocity retardation near the axis can be expected to lead to earlier vortex stagnation and

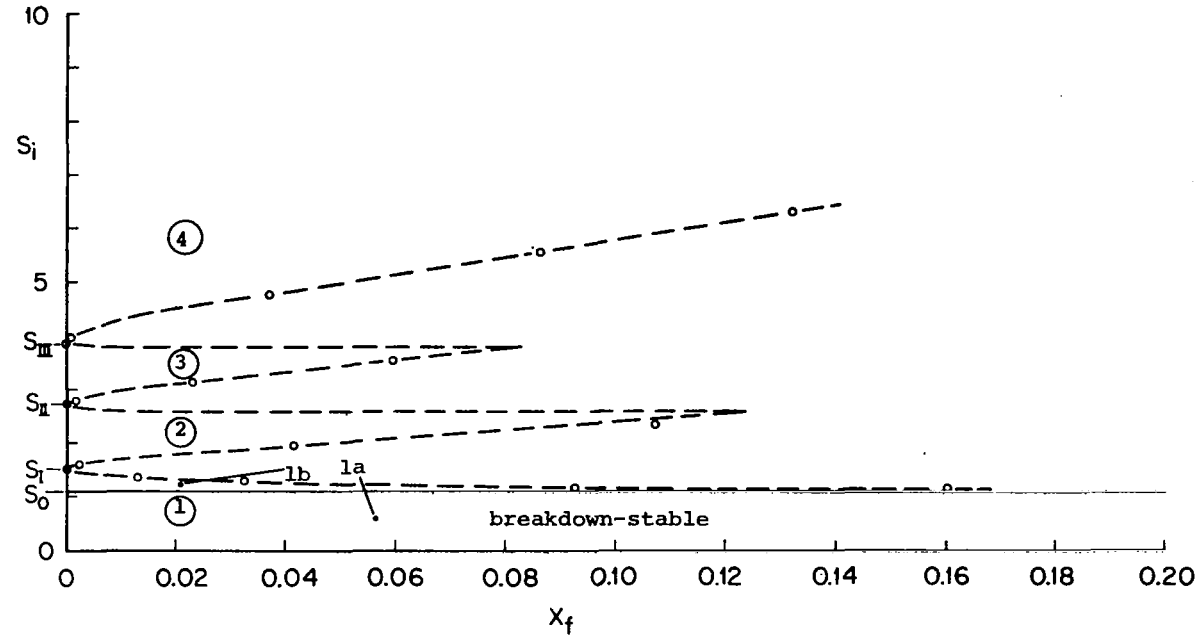

Fig. 4.2 Distance to failure (at X_f) as function of initial swirl parameter. Initial profiles of leading edge vortex type. Open circles denote failure of computation.

breakdown (see Sec. III).

The initial profile chosen was

$$U(Y) = 1 - e^{-Y}/2 \qquad \text{(i.e. } U_{ax} = 0.5,\ U_e = 1.0\text{)}$$

$$K(Y) = K_e(1 - e^{-Y})$$

For these profiles, external circulation and swirl values are related by

$$S = .792\ K_e/U_{ax} = .792\ K_e/0.5 = 1.584\ K_e$$

This choice appears to come fairly close to actual trailing vortex flows (McCormick et al. 1968).

Distances to failure of the computation at X_f for N = 3 are shown in Fig. 4.3 as a function of the initial swirl parameter. Again the behavior of the solutions is qualitatively the same as for the two previous cases. The actual critical swirl parameter

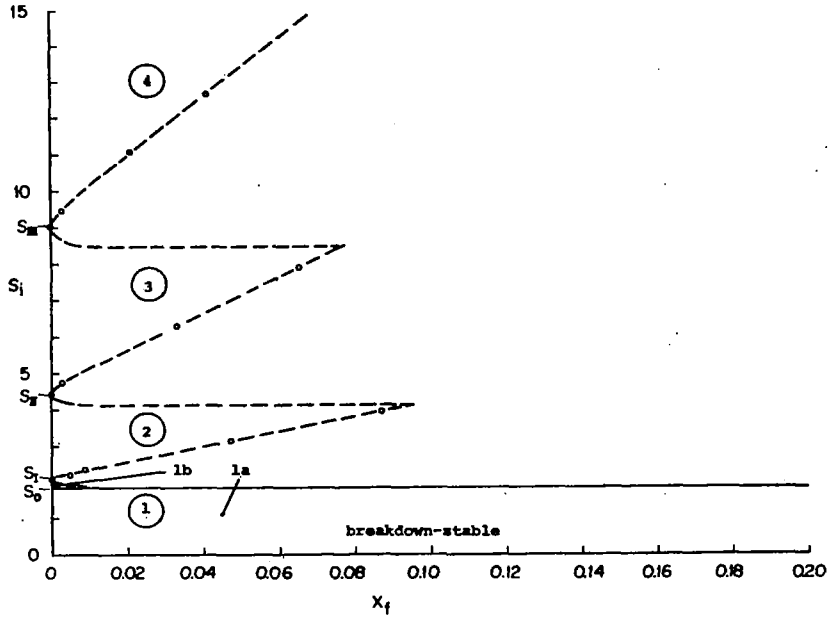

Fig. 4.3 Distance to failure (at X_f) as function of initial swirl parameter. Initial profiles of trailing vortex type. Open circles denote failure of computation.

values differ somewhat from the other two cases and again are not as accurate as those found in Sec. III for N = 5, especially for $S > S_2$.

Possibility of breakdown-stable solutions of type 2, 3, 4, ...

No breakdown-stable solutions of type 2, 3, or 4 were found in the present investigation for constant external axial velocity and circulation. This agrees with the results of the singularity analysis in Sec. III where it became evident that only specific external axial velocity and circulation gradients can prevent flows of these types from approaching a singularity. It will again be shown in Sec. V in several examples that application of external axial velocity or circulation gradients can have beneficial effects on flow development for these types. There is some other experimental and analytical evidence (Donaldson and Sullivan 1960) suggesting breakdown-stable solutions of the multi-layered type.

4.2 Velocity on the Axis

The behavior of vortex flow is different for each of the regions 1a, 1b, 2, 3, ... The most important indicator of vortex behavior is a plot of velocity on the axis U_{ax} vs. distance X. The development of the velocity on the axis will now be discussed for flows with constant external axial velocity and circulation. Before describing in greater detail flows of type 1 having different initial profiles, behavior of initially uniform axial flows of the first five types will be discussed. All results were computed with N = 3.

Behavior of initially uniform axial flows of types 1-4

Figure 4.4 presents the development of velocity on the axis in the five regions 1a, 1b, 2, 3, and 4. Each of the curves is representative of other flows in the same region. For flows of a given type, the character of these curves, and of the velocity profiles, remains the same. Type 1a, the only breakdown-stable

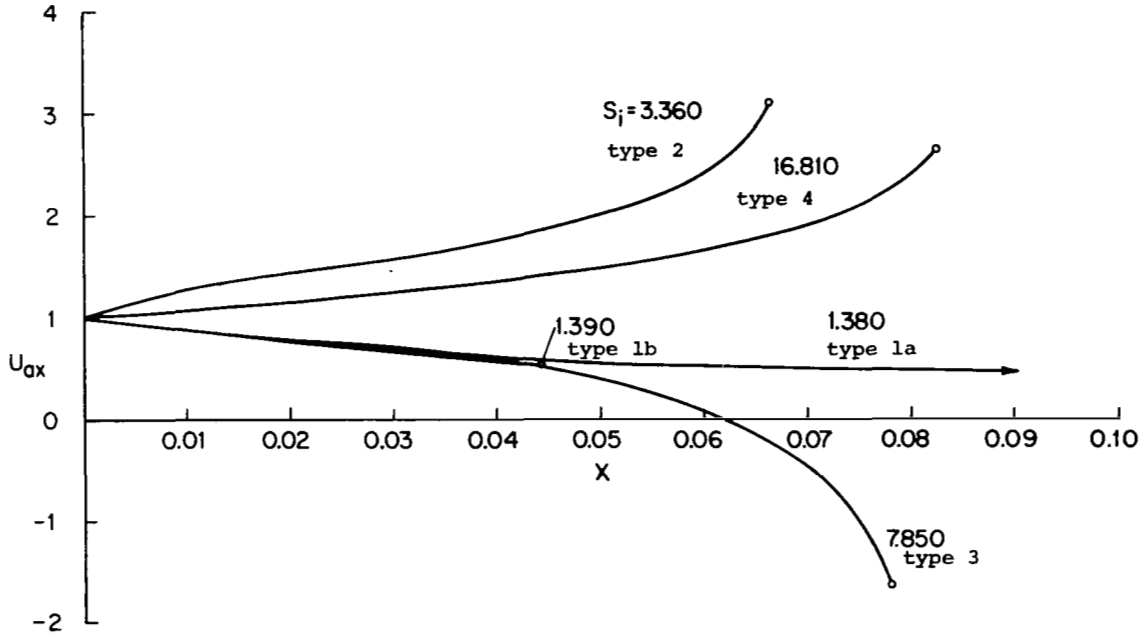

Fig. 4.4 Development of velocity on the axis for different flow types. Initially uniform axial flow. Open circles denote failure points.

flow, develops a reduc velocity on the axis which remains approximately constant for a considerable distance before it again approaches the freestream value. Type 1b flow has gradients (dU_{ax}/dX) which are always steeper than any type 1a gradients. These gradients increase, and the computation terminates due to excessive gradients, with U_{ax} in the neighborhood of 0.5. At the same time, the stream surface angles suddenly increase to large positive values, indicating an explosive behavior of the core. Gradients become larger, and the calculation breaks down increasingly sooner, as the critical swirl value S_1 is approached.

For swirl values greater than S_1, solutions of type 2 are obtained, which now show an acceleration of the velocity on the axis. Gradients (dU_{ax}/dX) are very large for S near S_1, but decrease as S is increased, leading to longer calculations before failure occurs. Failure of type 2 is an implosive one: stream surface angles assume large negative values very quickly in the immediate vicinity of the failure point. Gradients decrease further with correspondingly longer resulting computations, until the vicinity of S_2 is reached, where again no solutions can be obtained.

For swirl $S > S_2$, the flow is again of different type 3. The velocity on the axis now again decelerates, eventually reaching a stagnation point on the axis. Downstream of this point reversed flow develops on and near the axis, gradients steepen and computation fails with explosive behavior of the outer core. As the swirl is further increased, gradients are again reduced, and the computations fail farther downstream until the vicinity of S_3 is reached. No solutions can be obtained in the immediate neighborhood of this point.

For swirl $S > S_3$, the flow has once again changed its behavior (to type 4 flow). The velocity on the axis again tends to increase, until gradients again steepen rapidly, leading to

large negative stream surface angles in the outer core regions (implosive behavior), and the computation fails.

As S is increased, more and more singularities are encountered. The velocity on the axis alternates between a decelerating tendency (for odd type flow) and an accelerating tendency (for even type flow).

Initially uniform axial flow of type 1

Probably the only vortex flow of major physical significance is type 1 flow. The development of its velocity on the axis and its swirl parameter S(X) will now be given in more detail for the vortex with initially uniform axial flow.

Figure 4.5 presents results for different choices of initial swirl parameter S_i. It also gives the swirl parameter S(X) for two neighboring flows of type 1a and 1b. A swirl parameter value of approximately $S_i = 1.4$ separates the smoothly decaying vortex flows (type 1a: $S_i \lesssim 1.4$) from vortex flows which

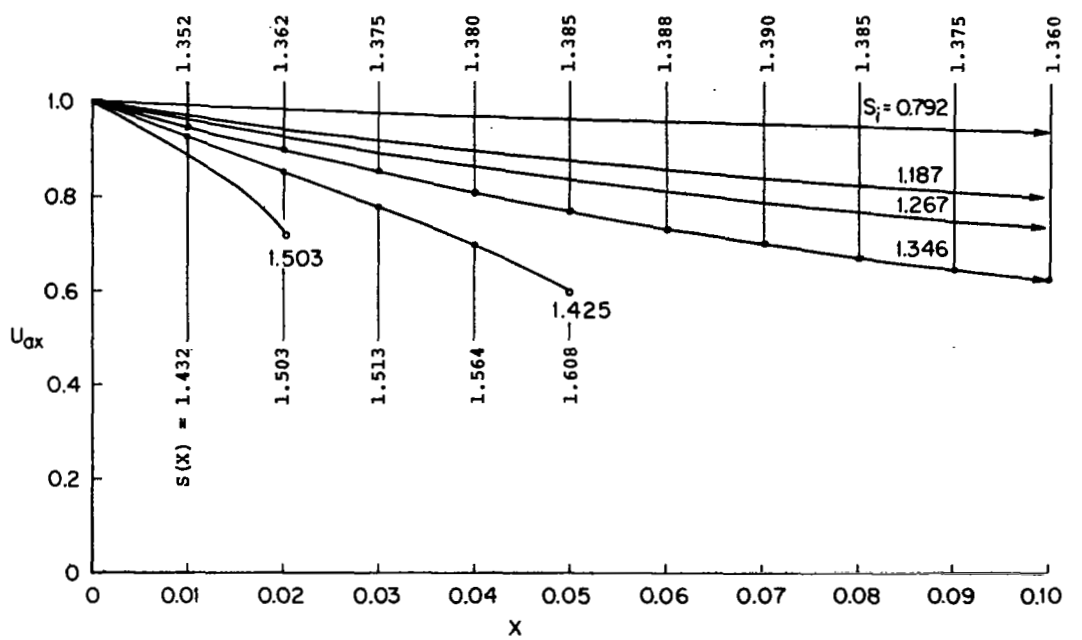

Fig. 4.5 Development of velocity on the axis as a function of initial swirl. Initially uniform axial flow. Open circles denote failure of the computation.

eventually break down (type 1b: $S_i \gtrsim 1.4$). Note that the theoretical inviscid value for the initial swirl value leading to stagnation is $S_i > \sqrt{2} = 1.41$ for rigid rotation (Bossel 1968).

Type 1a flow adjusts to an almost constant value of axial velocity and thereafter behaves in a wake-like manner. The swirl parameter S(X) generally decreases. The swirl still counteracts the normal spreading of the wake and the attendant diminishing of the axial velocity deficit; but eventually the axial velocity deficit again decreases, and the axial and swirl velocity profiles decay together.

Flows of type 1b initially behave much like those of type 1a, except that their rate of decrease of U_{ax} is steeper, and the swirl parameter S(X) increases. Eventually the swirl effects overwhelm the restoring tendencies of the wake, the drop of velocity on the axis steepens rapidly, and the computation fails. As an initial swirl parameter value of $S_i \approx 1.8$ is approached, the computation fails increasingly sooner. No solutions can be obtained near this point, whose theoretical inviscid value is $S_i = 3.8317/2 = 1.9159$ for rigid rotation (Fraenkel 1956).

Leading edge vortex of type 1

The development of the velocity on the axis for different initial swirl parameters S_i for a vortex of leading edge type (initially $U_{ax} = 2$, $U_e = 1$) is given in Fig. 4.6. The swirl parameter S(X) is also shown for two neighboring flows of type 1a and 1b. The behavior is qualitatively again the same as for the vortex with initially uniform axial velocity. A swirl parameter value of $S_i = 1.1$ divides the smoothly decaying type 1a from the breakdown type 1b. This value of S_i is somewhat lower than the theoretical value $S_o = \sqrt{2}$ for inviscid flow in rigid rotation and appears to reflect the influence of the profile shape. One would expect that the regions adjacent to the axis, where the axial velocity is lower, would have some

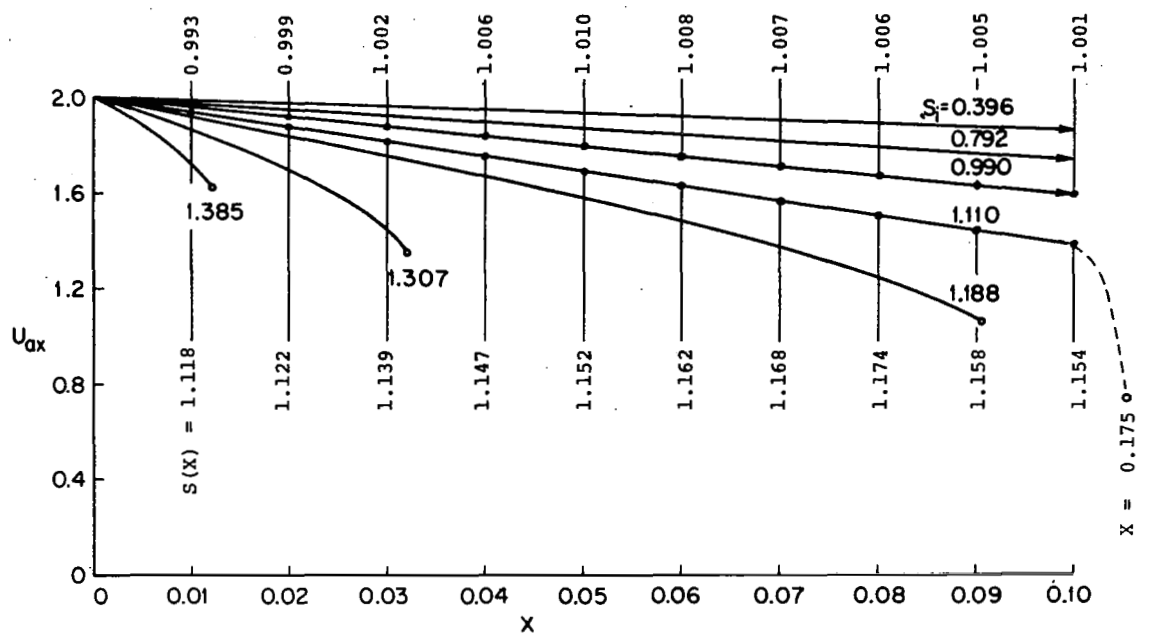

Fig. 4.6 Development of velocity on the axis as a function of initial swirl. Initial flow of leading edge vortex type. Open circles denote failure of the computations.

effect on the flow behavior and would therefore tend to bring down the critical value of S_i.

Trailing vortex of type 1

The development of velocity on the axis for different initial swirl parameters S_i for a trailing vortex (initially $U_{ax} = 0.5$, $U_e = 1$) is plotted in Fig. 4.7. The swirl parameter S(X) is also given for two neighboring flows of type 1a and 1b. The dividing value S_o of the initial swirl parameter is now greater than $\sqrt{2}$, reflecting again the influence of the nonuniform initial axial velocity profile.

4.3 Velocity Profiles

Figure 4.8 presents typical velocity profiles for initially uniform axial flow and N = 3 as they develop in the different swirl regions. The swirl velocity profile is hardly affected, but the axial velocity profile shows characteristic features

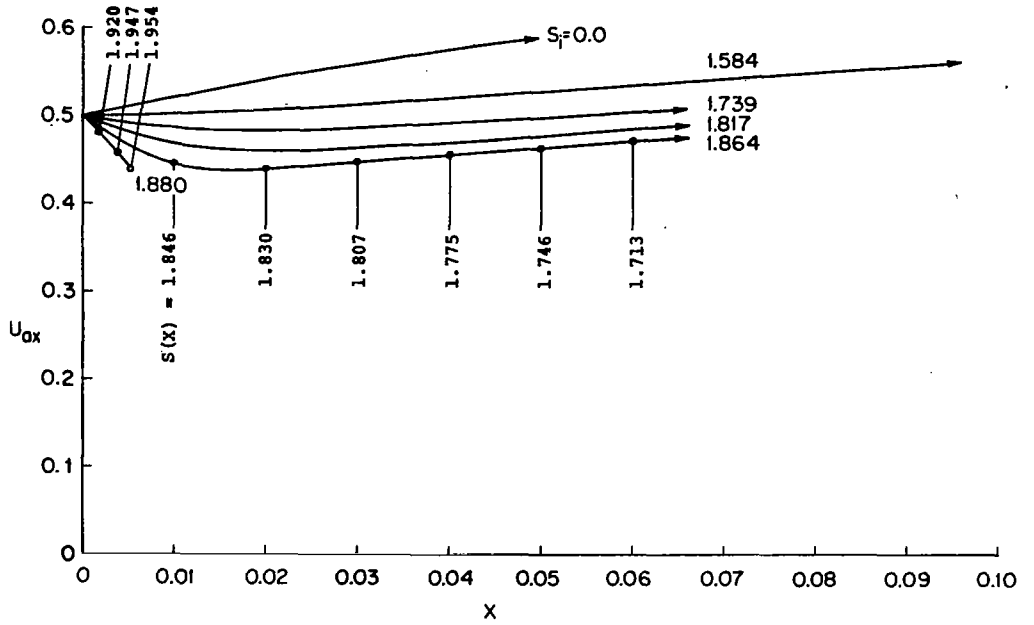

Fig. 4.7 Development of velocity on the axis as a function of initial swirl. Initial flow of trailing vortex type. Open circle denotes failure point.

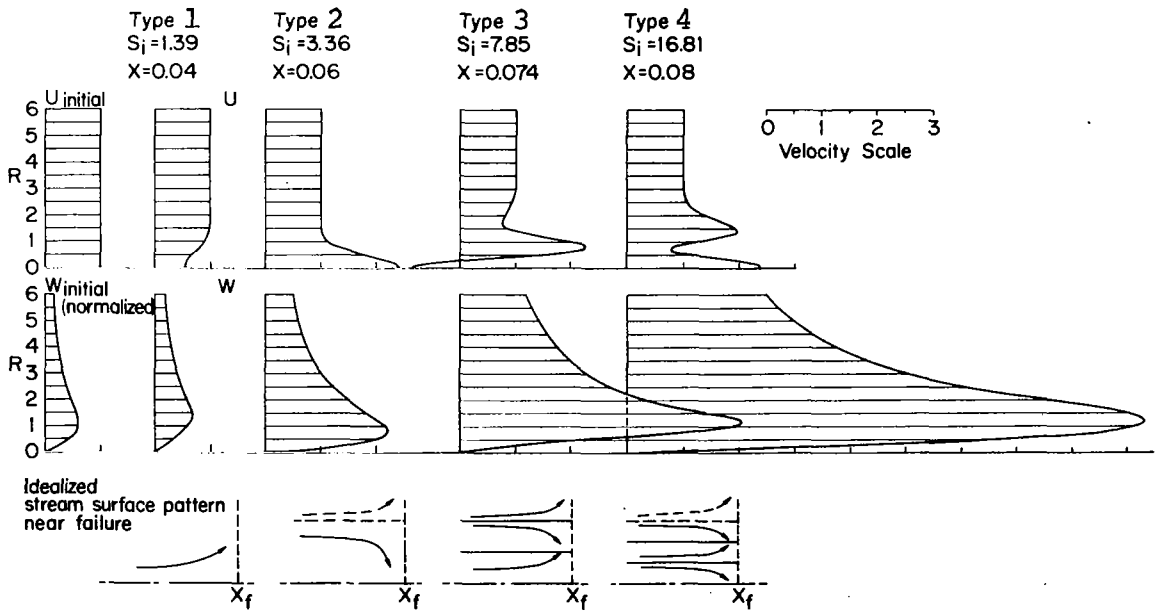

Fig. 4.8 Velocity profile development and flow character for different flow types. Initially uniform axial flow.

which are different in each region. Axial velocity profiles for these types, and for the initial profiles with uniform axial velocity, and leading edge vortex and trailing vortex character are given in more detail below.

For initially uniform axial flow a type 1 vortex always shows a decrease of velocity on the axis while in type 2 flow, the increase in velocity on the axis appears, as noted earlier. In addition, flow in a layer adjacent to the core may now be retarded, and the vortex may assume a two-layer structure. Similarly, in type 3 flow, three layers appear: a retarded core flow, an adjacent accelerated layer, and again, an outer retarded layer. In type 4 flow, four similar layers appear, with core flow being accelerated. This core structure has been qualitatively confirmed by calculations for different numbers of parameters N in the integral method of solution.

The velocity profile development for a smoothly decaying type 1a vortex with initially uniform axial flow is shown in Fig. 4.9. Behavior of type 1b flow is qualitatively similar up to the failure point. The swirl velocity profile shows a gradual decay, while the effect on the axial velocity profile (axial velocity retardation on and near the axis) is more pronounced and increases with swirl. Figures 4.10, 4.11, and 4.12 show the development of velocity profiles ($\gamma = 2$) when the initial swirl parameter S_i exceeds S_1. These three cases of types 2, 3, and 4 are representative of families of solutions between singularities S_1 and S_4. These solutions develop a multi-layer structure, and the core flow reacts differently in each family (i.e. acceleration or deceleration on the axis). All of these cases eventually fail.

Figure 4.13 shows the development of the axial and swirl velocity profiles for a (breakdown) type 1b flow of leading edge vortex type. Again there is a strong retarding effect on the axial velocity on and near the axis, while the swirl velocity profile is not greatly affected.

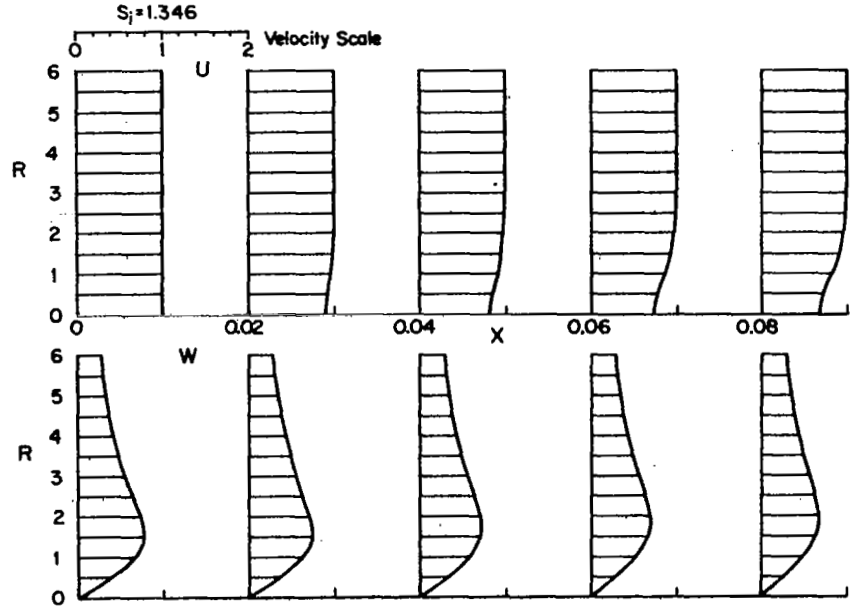

Fig. 4.9 Velocity profile development for initially uniform axial flow. Type 1a.

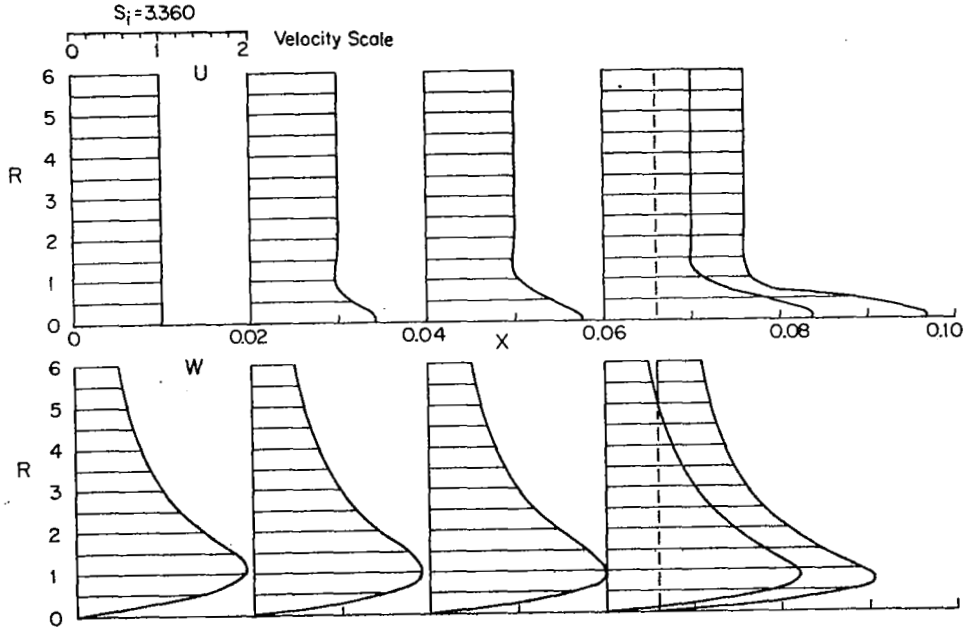

Fig. 4.10 Velocity profile development for initially uniform axial flow. Type 2.

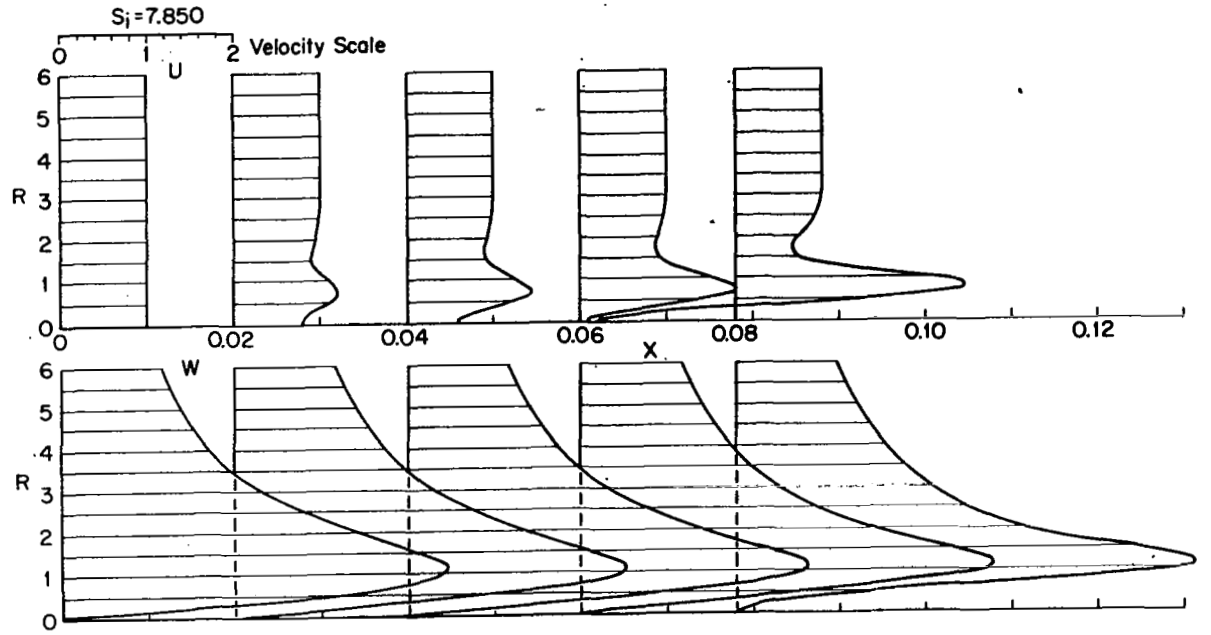

Fig. 4.11 Velocity profile development for initially uniform axial flow. Type 3.

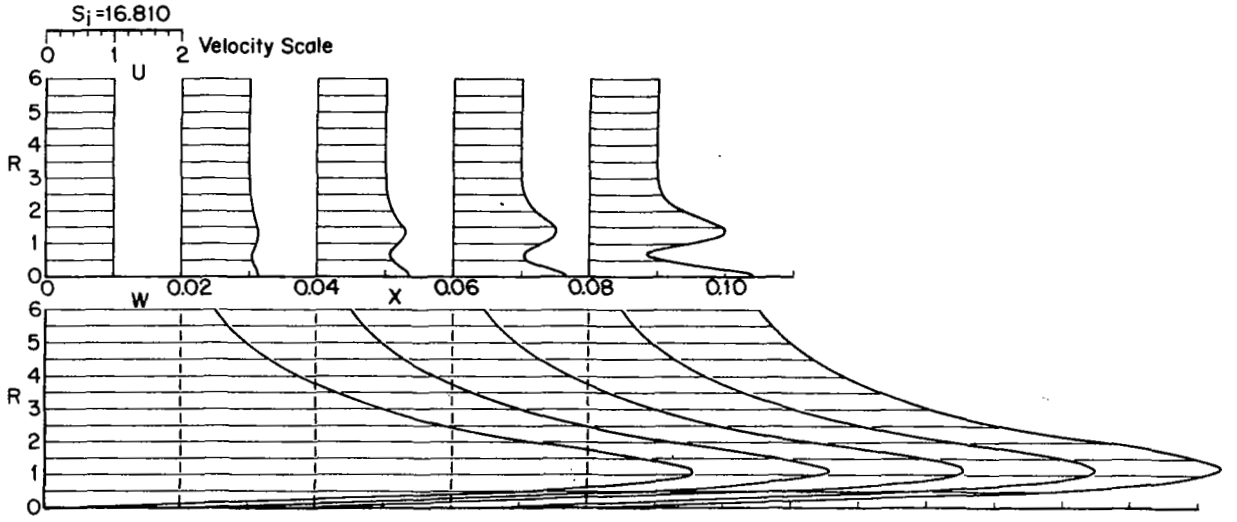

Fig. 4.12 Velocity profile development for initially uniform axial flow. Type 4.

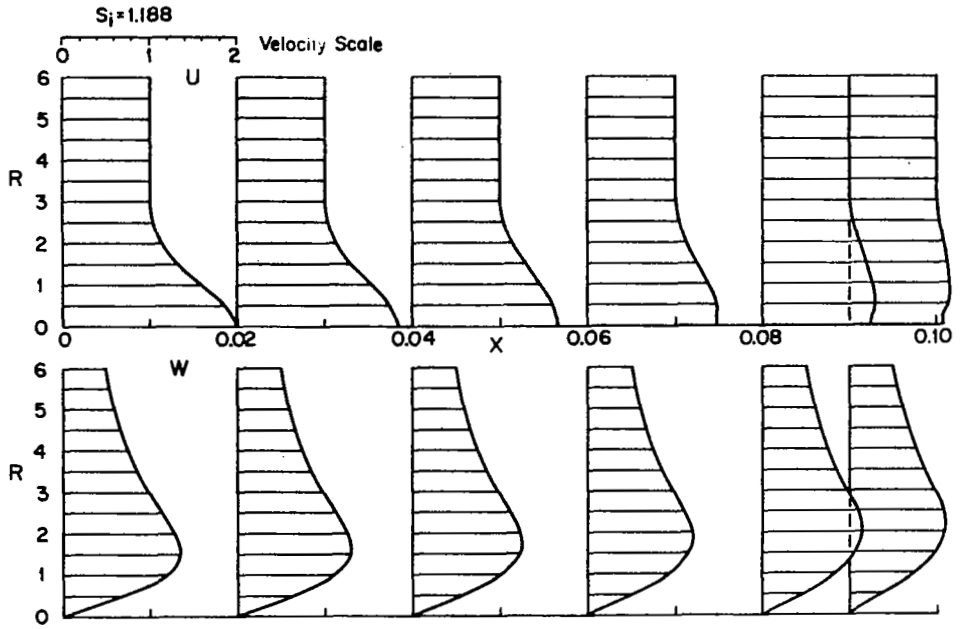

Fig. 4.13 Velocity profile development for initial flow of leading edge vortex type. Type 1b.

Figure 4.14 presents the development of axial and swirl velocity profiles for smoothly decaying type 1a flow of trailing vortex type.

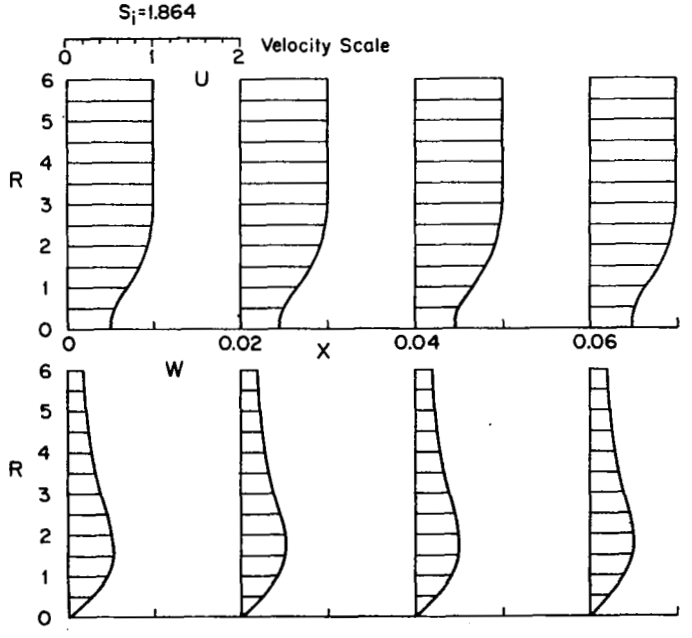

Fig. 4.14 Velocity profile development for initial flow of trailing vortex type. Type 1a.

V. EFFECTS OF EXTERNAL VELOCITY AND CIRCULATION DISTRIBUTION

The strong effects of external axial pressure gradients on vortex flows are well established experimentally (Lambourne and Bryer 1961, Harvey 1962, Hall 1966a) and in numerical computations (Hall 1966b, Mager 1971). A positive external velocity gradient has an accelerating effect on the axial velocity on and near the axis in type 1 vortex flows, thus decreasing the local swirl parameter and delaying or preventing breakdown. The effects of circulation gradient are less obvious. Combined external axial velocity and circulation effects may reinforce or cancel each other, depending on sign and magnitude of each and on the type of vortex flow. It will be shown here that external axial velocity and circulation gradients have contrasting effects on flows of different type. Such gradients can be used to prevent vortex breakdown, at least for some distance.

The behavior of vortex flows under external velocity and circulation gradients is of considerable interest in cases where breakdown of vortex flows is to be prevented or induced. Computation by methods such as the present one can indicate what velocity and circulation gradients should be applied and where.

5.1 Type 1 Vortex Flow

Type 1 flow is of considerable interest because it is the most common type in applications. Leading edge and trailing vortices on wings are usually of the breakdown-stable type 1a, but may change to stagnating type 1b as a result of either higher swirl (increased wing angle of attack) or adverse pressure gradient (negative external axial velocity and/or external circulation gradient).

External axial velocity and circulation gradients are felt through their effects on both the external pressure distribution

and the swirl parameter. The Bernoulli equation for the free-stream

$$p_o - p_e = (\rho/2)(u_e^2 + v_e^2 + (k_e/r)^2)$$

$$\approx (\rho/2)(u_e^2 + (k_e/r)^2)$$

shows the same qualitative effect of external axial velocity and circulation gradients on the pressure gradient. There is an amplified response of the flow on and near the axis to external pressure gradient (see Hall 1966a, p. 69) which is confirmed by all the present computations. Thus positive external axial velocity and circulation gradients will partly tend to cause increasing velocity on the axis for type 1 flow.

Flow behavior is governed by the swirl parameter $S \sim K_e/U_{ax}$. While the effect of positive external axial velocity and circulation gradients increases U_{ax} and decreases S, a circulation gradient also increases K_e and may raise S. A positive external velocity gradient is therefore always stabilizing in type 1 flow, while a positive external circulation gradient may be either stabilizing (in type 1a flow), or destabilizing (in type 1b flow), depending on which effect dominates.* The results presented here are for type 1 vortex flows with initially uniform axial velocity. Other initial axial velocity distributions give qualitatively the same result.

Figure 5.1 presents the results of the application of various positive and negative external axial velocity gradients to a type 1b vortex flow of fixed initial swirl and with initially uniform axial velocity. This particular flow breaks down under zero external velocity gradient. The same qualitative behavior is found for a type 1a vortex flow. The experimental

---

* 'Stabilization' is here taken to mean the prevention of axisymmetric vortex breakdown by avoiding any of the singularities S_1, S_2, ...

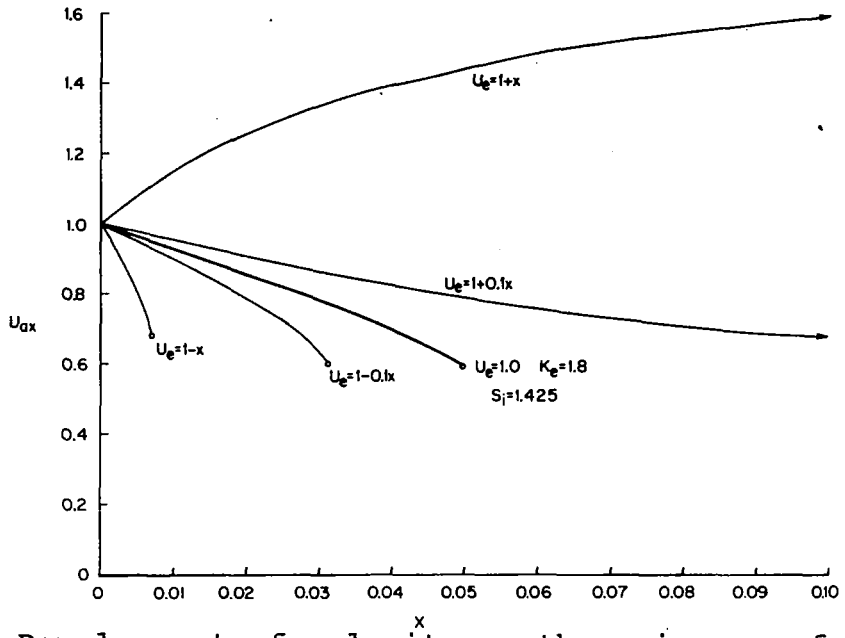

Fig. 5.1 Development of velocity on the axis as a function of external axial velocity gradient. Initially uniform axial flow of type 1b with S_i = 1.425 and K_e = 1.8 = const.

observations (breakdown delay or avoidance through a positive external axial velocity gradient) are confirmed, and the figure also illustrates the significant effect which even very small external velocity gradients can have on the velocity on the axis. Negative velocity gradients lower the critical swirl value and cause type 1b flow to break down sooner. Note that a positive velocity gradient can prevent breakdown and convert a flow from type 1b to 1a, even though the initial profile would indicate breakdown in a zero velocity gradient.

Figure 5.2 presents results of the application of different circulation gradients to a type 1a vortex. The effect of a moderate positive circulation gradient is qualitatively the same as for a positive velocity gradient. However, the effect reverses in type 1b flow (Fig. 5.3). Here a positive external circulation gradient results in earlier failure, while a negative gradient may prevent failure altogether. Note that this reversal of the circulation gradient effect can be used to

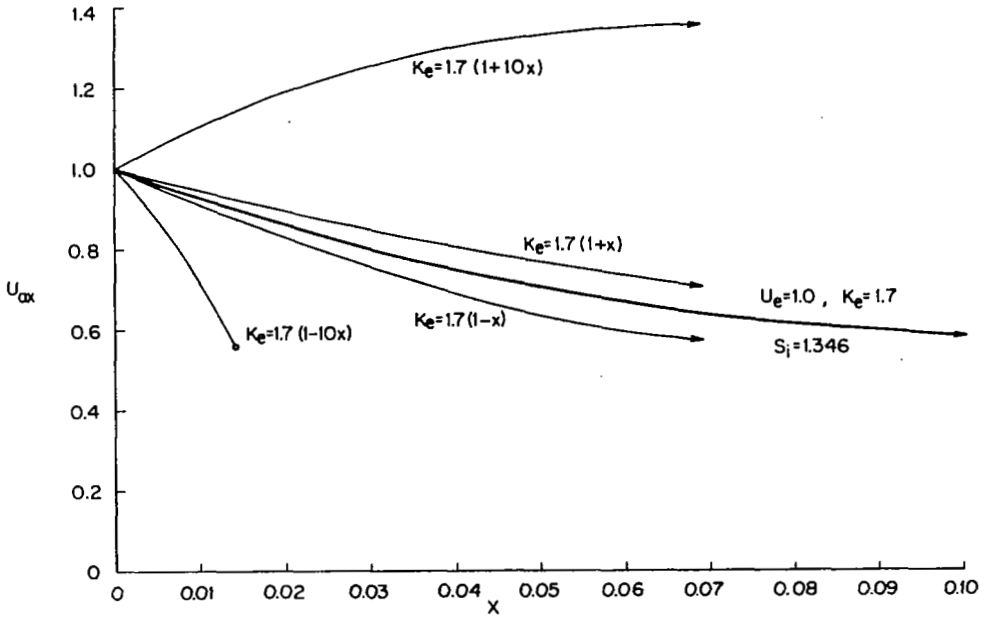

Fig. 5.2 Development of velocity on the axis as a function of external circulation gradient. Initially uniform axial flow of type 1a with S_i = 1.346 and U_e = 1.0 = const.

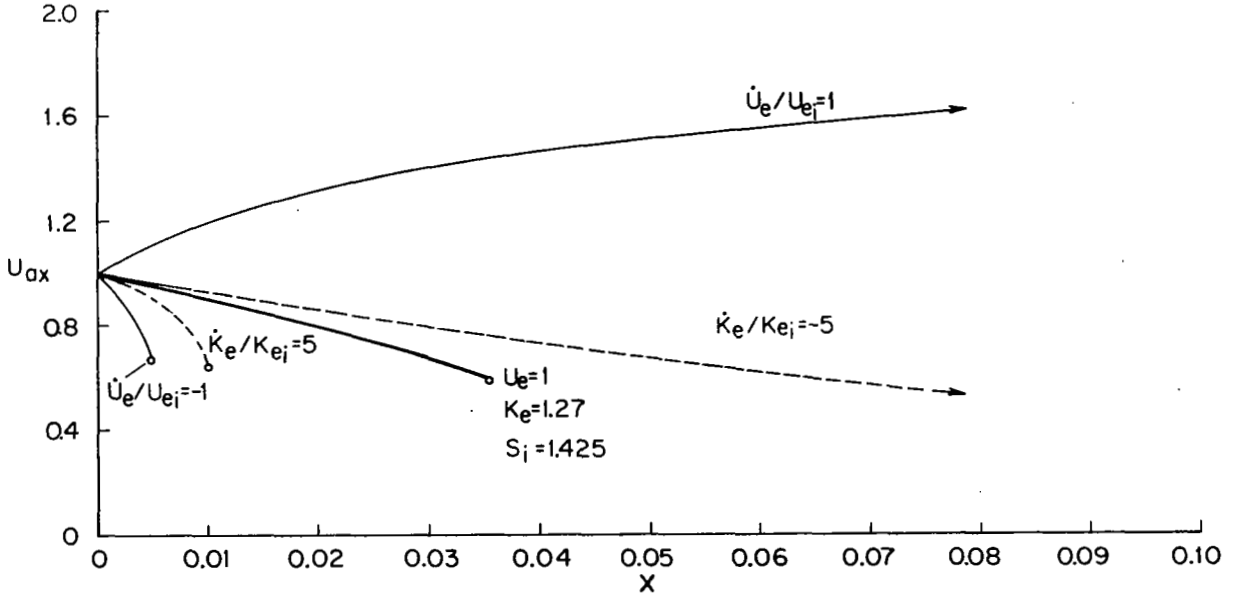

Fig. 5.3 Development of velocity on the axis for type 1b flow under different external axial velocity and circulation gradients. Initially uniform axial flow. U_{e_i} = 1.0, K_{e_i} = 1.27, S_i = 1.425.

— U_e = const, K_e = const; — U_e = variable, K_e = const; -- U_e = const, K_e = variable.

determine the critical value S_o separating wake-type (1a) from breakdown-type (1b) behavior.

5.2 Type 2 Vortex Flow

The effects of external axial velocity and circulation gradients on a type 2 vortex with initially uniform axial flow are illustrated in Fig. 5.4. For zero gradients the velocity on the axis would accelerate, eventually resulting in implosive failure, as noted earlier. A positive external axial velocity gradient accelerates the increase in velocity on the axis and the subsequent failure. A positive velocity gradient applied farther downstream has a retarding effect, however. A negative external axial velocity gradient initially causes a slower increase in velocity on the axis, but subsequently the slope begins to steepen, and (implosive) breakdown occurs earlier than with zero external velocity gradient.

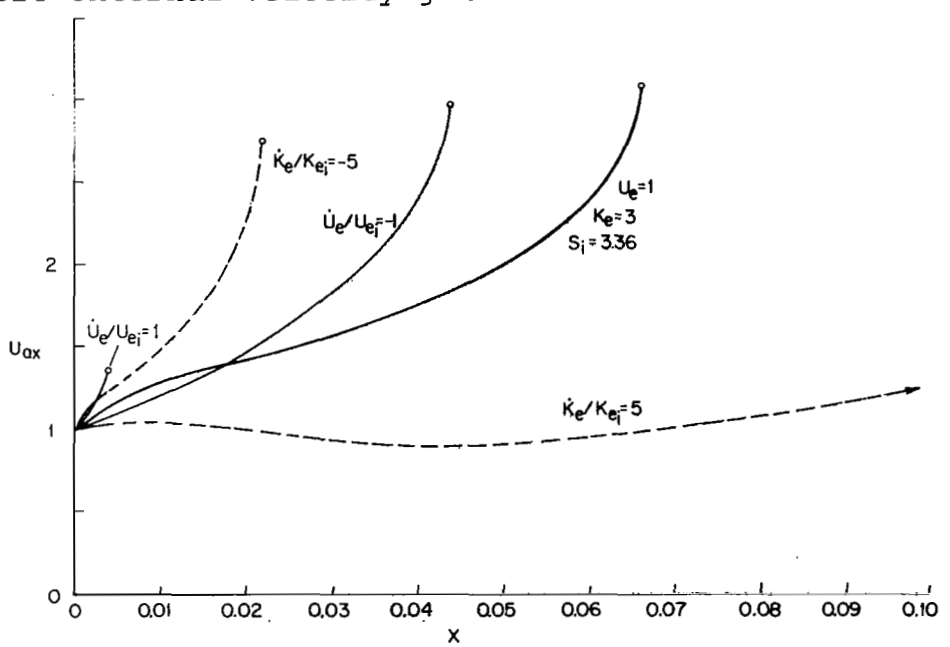

Fig. 5.4 Development of velocity on the axis for type 2 flow under different external axial velocity and circulation gradients. Initially uniform axial flow. $U_{e_i} = 1.0$, $K_{e_i} = 3.0$, $S_i = 3.36$.
— U_e = const, K_e = const; — U_e = variable, K_e = const; – – U_e = const, K_e = variable.

A positive external circulation gradient hinders the acceleration of velocity on the axis. It may even keep the velocity on the axis approximately constant and suppress the development of extreme velocity peaks in the axial velocity profile, thus stabilizing the vortex for considerable distance. However, in such cases, the velocity on the axis shows a divergent oscillatory behavior, and eventual (implosive) failure must be expected. Negative external circulation gradients lead to further acceleration of the velocity on the axis and to earlier failure.

5.3 Type 3 Vortex Flow

A type 3 vortex with initially uniform axial flow and zero external gradient shows a velocity retardation on the axis which leads to eventual stagnation there and an inner region of reversed axial flow surrounded by an annular region where the axial velocity exceeds the freestream velocity. Failure eventually results. Figure 5.5 presents the results of external axial velocity and circulation gradients on this flow.

A positive external axial velocity gradient causes further deceleration of the velocity on the axis and an earlier failure. A negative gradient accelerates the velocity on the axis and may retard failure for a significant distance.

A positive external circulation gradient has the same effect as a positive velocity gradient, and it usually leads very quickly to a drop in the velocity on the axis and to failure. A negative external circulation gradient, if strong enough, will accelerate the velocity on the axis and lead to implosive failure.

5.4 Type 4 Vortex Flow

A type 4 vortex with initially uniform axial flow and zero external axial velocity or circulation gradients shows increasing velocity

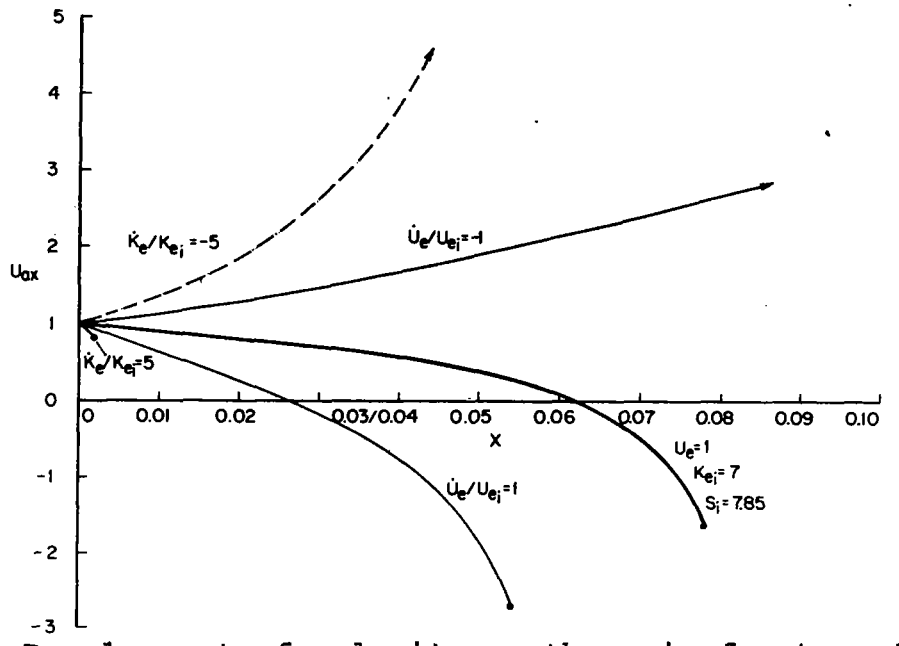

Fig. 5.5 Development of velocity on the axis for type 3 flow under different external axial velocity and circulation gradients. Initially uniform axial flow. $U_{e_i} = 1.0$, $K_{e_i} = 7.0$, $S_i = 7.85$.
——U_e = const, K_e = const; —— U_e = variable, K_e = const;
——U_e = const, K_e = variable.

on the axis and, eventually, implosive failure of the inner core. The effect of applied external axial velocity and circulation gradients is shown in Fig. 5.6.

A positive external axial velocity gradient initially causes slower growth, or deceleration, of the velocity on the axis before U_{ax} again rises steeply and failure occurs. A negative external axial velocity gradient, while steepening the rise in velocity on the axis, may retard failure for a considerable distance.

A positive external circulation gradient can stabilize the flow for some distance. Again, however, a divergent oscillation appears in the velocity on the axis, leading to eventual failure. A negative external circulation gradient leads to quick acceleration of the velocity on the axis and to earlier failure.

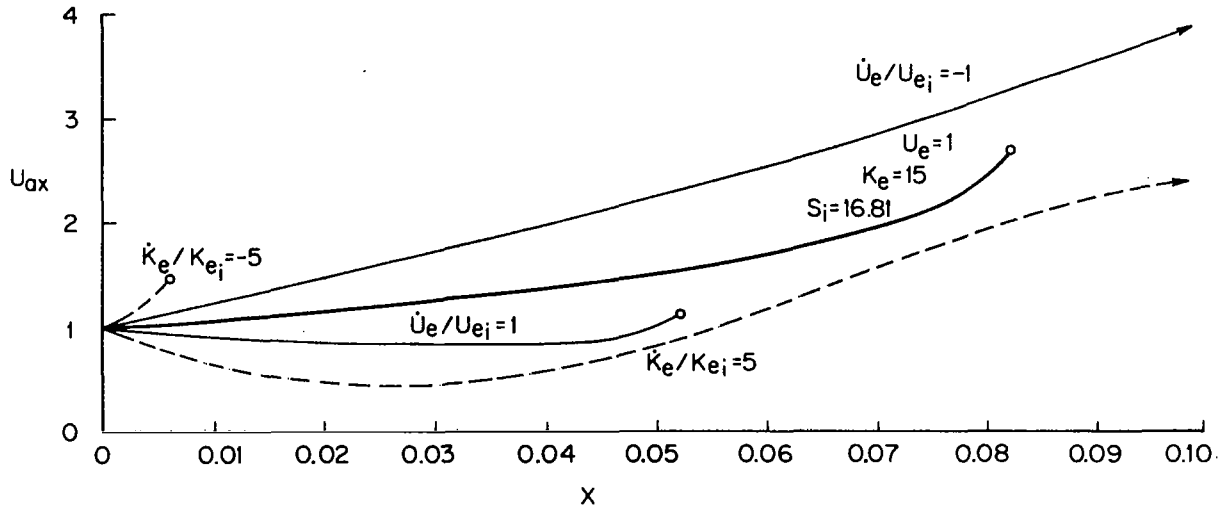

Fig. 5.6 Development of velocity on the axis for type 4 flow under different external axial velocity and circulation gradients. Initially uniform axial flow. $U_{e_i} = 1.0$, $K_{e_i} = 15.0$, $S_i = 16.81$. —— U_e = const, K_e = const; —— U_e = variable, K_e = const; – – U_e = const, K_e = variable.

5.5 Avoidance of Singularities

Table 5.1 summarizes the results of subsections 1 through 4. Note that the effects of gradients superimpose on the result for zero gradients, and that the net result may be an initial decrease and later increase in velocity on the axis, for example (as in some cases 4 with a positive external axial velocity gradient).

Material presented here has shown that (1) the core flow is mainly responsible for eventual failure, and that (2) the core flow is easily influenced by external flow conditions. It is therefore obviously possible to influence the development of all vortex types by application of external axial velocity or circulation gradients. A question of practical importance is whether such gradients can be used to stabilize vortex flows which are initially of unstable type. The singularity analysis of Sec. III indicates that this should be possible.

Table5.1

Behavior of Vortex Flows

Separating swirl parameter	0	S_o	S_1	S_2	S_3
Type (uniform initial axial flow)	1a	1b	2	3	4
Initial development for zero external axial velocity and circulation gradients: Velocity on axis	decreases		increases	decreases	increases
Positive external axial velocity gradient causes additional	acceleration		acceleration (later: deceleration)	decel.	deceleration
(Modest) positive external circulation gradient causes additional	accel.	decel.	deceleration	decel.	deceleration

Permanent stabilization of flow initially of type 1b by external axial velocity or circulation gradients can be achieved, as evidenced by Fig. 5.3 and supported by experimental evidence. As a further example, Fig. 5.7 demonstrates the result of application of a very small positive external axial velocity gradient on initially breakdown-unstable type 1b vortex flow. The gradient was applied at X_o in the immediate vicinity of the failure point, transforming the vortex into a breakdown-stable 1a type.

It has already been said (Sec. I) that application of the parabolic system (1) to subcritical vortex flow ($S > S_1$) is open to criticism, but results are nevertheless believed to describe trends correctly. The following discussion of behavior of flows in the subcritical region is based on the parabolic system and refers to behavior of corresponding solutions.

Since the parabolic system exhibits singularities (S_1, S_2,

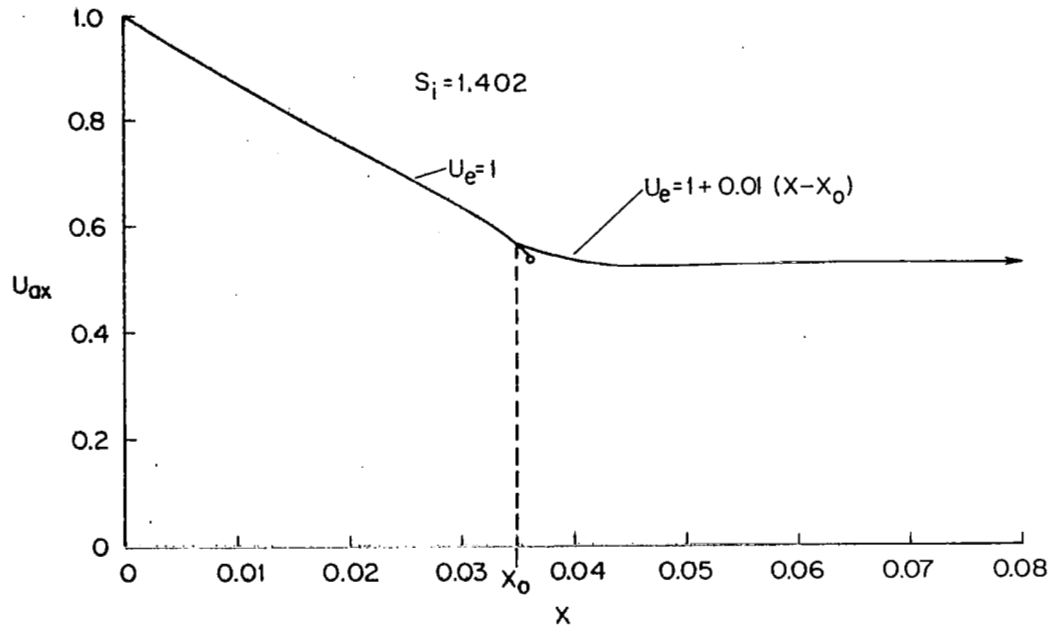

Fig. 5.7 Prevention of breakdown of type 1b flow by application of a small positive external axial velocity gradient beginning at X_o. Initially uniform axial flow, $S_i = 1.402$.

S_3, etc.) it will not be possible to go from one flow type to another without failure of the computation. In particular, it will not be possible to go from type 2, 3, or 4 flow to breakdown-stable type 1a flow without computational failure. Stabilization within a given flow type by application of external axial velocity and/or circulation gradients is another matter. Failure may be avoided for a considerable distance; and permanent stabilization appears possible by application of specific external axial velocity and circulation gradients (Sec. III). In applications, stable vortex flows are usually required only over finite distances, and application of favorable external axial velocity or circulation gradients can result in retarding failure for a sufficient distance, as shown in previous subsections.

Stable multi-layer vortex flows of high swirl $S > S_1$ do exist in nature (certain tornados and water spouts) and can be generated in the laboratory (Rosenzweig, Ross, Lewellen 1962).

Their correct and full treatment, beyond establishing general trends, appears to require more than a solution of the parabolic system (2.1).

VI. CONCLUSIONS

The computation of viscous quasi-cylindrical vortex flows at low swirl values does not present any particular difficulities and can be handled by methods which are only slightly more complicated than comparable methods of boundary layer computation. Computational difficulties arise at high swirl values due to the appearance of swirl- and profile-dependent singularities which indicate a failure of the quasi-cylindrical approximation and appear to correspond to physical axisymmetric 'vortex breakdown'.

On the basis of recent optical velocity measurements in vortex breakdown flows, a distinction has been made in this report in particular between 'vortex breakdown', 'vortex jump', and the 'vortex bubbles' assocated with vortex breakdown. While the vortex breakdown and vortex bubble flow must be computed by using the (elliptic) Navier-Stokes equation or the correct (inviscid) subset thereof, the flow approaching the breakdown can be computed by the (parabolic) quasi-cylindrical vortex equations used in this report. This set has been shown to have an infinite number of discrete singularities. A 'vortex jump' in the sense of Benjamin's (1962) hydraulic jump analogy may occur downstream of the vortex breakdown and vortex bubble. A solution in the jump region must include a proper matching condition between two conjugate flows.

The present report has presented

(1) an accurate and efficient method for the computation of viscous incompressible quasi-cylindrical axisymmetric steady vortex flow,

(2) a method for obtaining the singular swirl values for a given vortex velocity profile combination (axial velocity profile and swirl velocity profile, or circulation profile),

(3) results of vortex computations for a wide range of swirl parameters, initial profiles, and external axial velocity and circulation gradients.

The numerical method of integration of the vortex equations is an application of the method of weighted residuals. The present method uses exponentials in both the approximating expressions for axial velocity and circulation and as weighting functions. It is formulated for arbitrary N and can produce quick qualitative studies for N = 1 or 2, or more accurate results for N > 2. The results presented were for N = 3. Computation of a multitude of vortex flows has been efficient and virtually trouble-free. In exploratory investigations such as this one and in more detailed analyses of flows, the use of N-parameter integral methods appears to have distinct advantages and much potential. The singularities of a given vortex velocity profile combination were found by introducing its describing parameters into the set of equations for the parameter gradients and determining the swirl parameters for which the system becomes singular (and the gradients infinite).

Major results of the investigation were as follows:

(1) The equations of viscous quasi-cylindrical incompressible vortex flow have an infinite number of discrete singularities. These singularities are best categorized in terms of the swirl parameter of an equivalent cylinder of fluid in rigid rotation. For given vortex velocity profiles, the singular swirl parameter values can be computed to determine flow behavior, or results such as the present can be used as guidelines.

(2) The singular swirl parameters S_1, S_2, . . . appear to correspond to the critical values $j_{1n}/2$ of the swirl parameter in the solution of the equation of inviscid flow with initial rigid rotation. (The regions of validity of the viscous and inviscid sets overlap at and near the axis, but the viscous quasi-cylindrical set becomes invalid where stream surfaces

expand or contract rapidly.) The exact values of S_1, S_2, . . . are profile-dependent.

(3) At each singularity, all derivatives become infinite in magnitude and reverse their signs. The result is contrasting behavior of vortex flows on both sides of the singularity. In particular, as the first singularity S_1 is crossed from below (increasing swirl parameter), the tendency to deceleration of the velocity on the axis (and expansion of stream surfaces) changes to one of acceleration (and contraction).

(4) For swirl parameters less than a dividing value $S_o < S_1$, vortex flows show smooth viscous decay of all velocity profiles to the surrounding freestream velocity (type 1a). For swirl parameters greater than S_o, increasingly rapid deceleration on the axis develops, the swirl paramter S(X) increases further, and the computation fails when the singularity $S(X) = S_1$ is reached (type 1b). S_o is profile-dependent and appears to correspond to the dividing value $S_o = \sqrt{2}$ for inviscid flow in initially rigid rotation.

(5) External gradients of axial velocity or circulation can affect the swirl parameter S(X) and corresponding flow behavior by either speeding the approach to a singularity or by avoiding it altogether. In particular, breakdown-prone flows of type 1b with $S(X) > S_o$ can be transformed to type 1a, which will not break down. At the dividing point S_o, the effect of an external circulation gradient reverses.

(6) Each new singularity first enters at the axis and spreads outward as S is increased. This leads to alternately decelerating and accelerating layers in the axial flow profiles. Thus for $S_3 < S < S_4$ (type 4 flow), four layers exist: accelerating core-flow, adjacent decelerating layer, an accelerating layer next, and a decelerating outer layer. It does not appear that breakdown-stable vortex configurations are possible under these conditions for $S > S_o$, unless external axial velocity and

circulation gradients are applied.

(7) The singularities are coupled with explosive or implosive expansion, respective contraction of the stream surfaces, and the parabolic viscous subset of the Navier-Stokes equations used in the present work becomes invalid and should be replaced by the inviscid equations of rotating flow or by the full Navier-Stokes equations very close to and at the singularities (Bossel 1969). These sets permit continuous solutions for all S. The results presented here are valid almost to the point of computational failure in most cases since stream surface angles remain of the order of a few degrees for typical core Reynolds numbers of order 10^4.

(8) No qualitative difference exists in the behavior of flows of same type but having different velocity profiles (i.e. uniform initial axial flow, leading edge vortex, trailing vortex).

APPENDIX

Coefficients in the ordinary differential equations (2.5):

$$A_{n,k} = \sum_{\ell=1}^{N} a_\ell S_{1,k} + U_e S_{2,k} + U_{ax} S_{3,k}$$

$$B_{n,k} = \sum_{\ell=1}^{N} b_\ell Q_{1,1}/2 + K_e Q_{1,2}/2$$

$$C_k = \sum_{\ell=1}^{N} a_\ell S_{7,k} + U_e S_{8,k} + U_{ax} S_{9,k}$$

$$D_k = \sum_{\ell=1}^{N} a_\ell S_{4,k} + U_e S_{5,k} + U_{ax} S_{6,k}$$

$$E_k = \sum_{\ell=1}^{N} b_\ell Q_{1,4}/2 + K_e Q_{1,5}/2$$

$$F_k = \sum_{n=1}^{N} a_n T_{1,k} + U_e T_{2,k} + U_{ax} T_{3,k}$$

$$\bar{A}_{n,k} = \sum_{\ell=1}^{N} b_\ell \bar{S}_{1,k} + K_e \bar{S}_{2,k}$$

$$\bar{B}_{n,k} = \sum_{\ell=1}^{N} a_\ell Q_{1,1} + U_e Q_{1,2} + U_{ax} Q_{1,3}$$

$$\bar{C}_k = \sum_{\ell=1}^{N} b_\ell \bar{S}_{7,k} + K_e \bar{S}_{8,k}$$

$$\bar{D}_k = \sum_{\ell=1}^{N} b_\ell \bar{S}_{4,k} + K_e \bar{S}_{5,k}$$

$$\bar{E}_k = \sum_{\ell=1}^{N} a_\ell Q_{1,4} + U_e Q_{1,5} + U_{ax} Q_{1,6}$$

$$\bar{F}_k = \sum_{n=1}^{N} b_n \bar{T}_{1,k} + K_e \bar{T}_{2,k}$$

These coefficients involve present values of the parameters a_n, b_n, and of U_{ax}, U_e, and K_e. They must therefore be calculated anew at each step. However, the numbers Q, S, T, $\bar{S}$, and $\bar{T}$ are constants which are determined only once at the beginning of the computation. It is convenient to define them in terms of other constants Z, P, and R. The following numbers are all for given ℓ and n. The index k runs from 1 to N + 1.

Let

$$Z_{1,1} = \sigma_k^{-1}$$

$$Z_{2,1} = (\sigma_k + \alpha)^{-1}$$

$$Z_{3,1} = (\sigma_k + 2\alpha)^{-1}$$

$$Z_{4,1} = (\sigma_k + n\alpha)^{-1}$$

$$Z_{5,1} = [\sigma_k + (n + 1)\alpha]^{-1}$$

$$Z_{6,1} = [\sigma_k + (n + 2)\alpha]^{-1}$$

$$Z_{7,1} = [\sigma_k + (n + \ell)\alpha]^{-1}$$

$$Z_{8,1} = [\sigma_k + (n + \ell + 1)\alpha]^{-1}$$

$$Z_{9,1} = [\sigma_k + (n + \ell + 2)\alpha]^{-1}$$

$$Z_{10,1} = [\sigma_k + \ell\alpha]^{-1}$$

$$Z_{11,1} = [\sigma_k + (\ell + 1)\alpha]^{-1}$$

$$
\left.
\begin{aligned}
Z_{12,1} &= [\sigma_k + (\ell + 2)\alpha]^{-1} \\
Z_{i,2} &= Z_{i,1}Z_{i,1} \\
Z_{i,3} &= 2Z_{i,2}Z_{i,1} \\
Z_{i,4} &= 3Z_{i,3}Z_{i,1}
\end{aligned}
\right\} \quad i = 1, 2, \ldots, 12
$$

Then

$$
\left.
\begin{aligned}
P_{m,1} &= Z_{4,m} - Z_{5,m} \\
P_{m,2} &= Z_{1,m} - Z_{2,m} \\
P_{m,3} &= Z_{2,m}
\end{aligned}
\right\} \quad m = 1, 2, 3, 4
$$

For the Q's and R's the index m = 1, 2, 3:

$$Q_{m,1} = Z_{7,m} - 2Z_{8,m} + Z_{9,m}$$

$$Q_{m,2} = Z_{4,m} - 2Z_{5,m} + Z_{6,m}$$

$$Q_{m,3} = Z_{5,m} - Z_{6,m}$$

$$Q_{m,4} = Z_{10,m} - Z_{11,m}$$

$$Q_{m,5} = Z_{1,m} - 2Z_{2,m} + Z_{3,m}$$

$$Q_{m,6} = Z_{2,m} - Z_{3,m}$$

$$Q_{m,7} = Z_{11,m} - Z_{12,m}$$

$$Q_{m,8} = Z_{2,m} - Z_{3,m}$$

$$Q_{m,9} = Z_{3,m}$$

$$R_{m,1} = (Z_{10,m} - Z_{8,m} - Z_{11,m} + Z_{9,m})/[(n + 1)\alpha] + (-Z_{10,m} + Z_{7,m} + Z_{11,m} - Z_{8,m})/(n\alpha)$$

$$R_{m,2} = (Z_{1,m} - Z_{5,m} - Z_{2,m} + Z_{6,m})/[(n+1)\alpha] + (-Z_{1,m} + Z_{4,m} + Z_{2,m} - Z_{5,m})/(n\alpha)$$

$$R_{m,3} = (Z_{2,m} - Z_{6,m})/[(n+1)\alpha] + (-Z_{2,m} + Z_{5,m})/(n\alpha)$$

$$R_{m,4} = (Z_{10,m} - 2Z_{11,m} + Z_{12,m})/\alpha - Z_{10,m+1} + Z_{11,m+1}$$

$$R_{m,5} = (Z_{1,m} - 2Z_{2,m} + Z_{3,m})/\alpha - Z_{1,m+1} - Z_{2,m+1}$$

$$R_{m,6} = (Z_{2,m} - Z_{3,m})\alpha - Z_{2,m+1}$$

$$R_{m,7} = (-Z_{10,m} + 2Z_{11,m} - Z_{12,m})/\alpha$$

$$R_{m,8} = (-Z_{1,m} + 2Z_{2,m} - Z_{3,m})/\alpha$$

$$R_{m,9} = (Z_{3,m} - Z_{2,m})/\alpha$$

Then

$$S_{i,k} = 2\sigma_k Q_{3,i} - 4Q_{2,i} + \sigma_k^2 R_{3,i} - 4\sigma_k R_{2,i} + 2R_{1,i}$$

$$\bar{S}_{i,k} = Q_{1,i} + \sigma_k R_{1,i} \qquad i = 1, 2, \ldots 9$$

$$T_{i,k} = -2\sigma_k^3 P_{4,i} + 14\sigma_k^2 P_{3,i} - 20\sigma_k P_{2,i} + 4P_{1,i}$$

$$\bar{T}_{i,k} = -2\sigma_k^2 P_{2,i} + 4\sigma_k P_{1,i} \qquad i = 1, 2, 3$$

REFERENCES

Batchelor, G. K. (1964): Axial Flow in Trailing Line Vortices. J. of Fluid Mech., 20, 4, pp. 645-658.

Benjamin, T. B. (1962): Theory of the Vortex Breakdown Phenomenon. J. Fluid Mech., 14, pp. 593-629.

Benjamin, T. B. (1967): Some Developments in Theory of Vortex Breakdown. J. Fluid Mech., 28, 1, pp. 65-84.

Bethel, H. E. (1968): Approximate Solution of the Laminar Boundary-Layer Equations with Mass Transfer. AIAA Journal, 6, 2, pp. 220-225.

Bossel, H. H. (1967): Inviscid and Viscous Models of the Vortex Breakdown Phenomenon. Rept. AS-67-14, College of Engineering, University of California, Berkeley, Calif.

Bossel, H. H. (1968): Stagnation Criterion for Vortex Flows. AIAA Journal, 6, 6, pp. 1192-1193.

Bossel, H. H. (1969): Vortex Breakdown Flowfield. Phys. of Fluids, 12, pp. 498-508.

Bossel, H. H. (1970a): Use of Exponentials in the Integral Solution of the Parabolic Equations of Boundary Layer, Wake, Jet, and Vortex Flows. J. Comp. Physics, 5, 3, pp. 359-382.

Bossel, H. H. (1970b): Boundary Layer Computation by an N-Parameter Integral Method Using Exponentials. AIAA Journal, 8, 10, pp. 1841-1845.

Bossel, H. H. (1971): Vortex Computation by the Method of Weighted Residuals Using Exponentials. AIAA Journal, 9, 10, pp. 2027-2034.

Burgers, J. M. (1940): Application of a Model System to Illustrate Some Points of the Statistical Theory of Free Turbulence. Proceedings of the Academy of Sciences, Amsterdam, Vol. 43, No. 1, pp. 2-12.

Chow, Chuen-Yen (1969): Swirling Flow in Tubes of Non-Uniform Cross-Sections. J. Fluid Mech., 38, 4, pp. 843-854.

Donaldson, C. duP. and Sullivan, R. D. (1960): Behavior of Solutions of the Navier-Stokes Equations for a Complete Class of Three-dimensional Viscous Vortices. Proc. of the Heat Transfer and Fluid Mechanics Institute, pp. 16-30.

Dorodnitsyn, A. A. (1962): General Method of Integral Relations and its Application to Boundary Layer Theory. Advances in Aeronautical Sciences, Vol. 3, Pergamon Press, New York, pp. 207-219.

Fraenkel, L. E. (1956): On the Flow of Rotating Fluid Past Bodies in a Pipe. Proc. Roy. Soc. A., 233, pp. 506-526.

Gartshore, I. S. (1963): Some Numerical Solutions for the Viscous Core of an Irrotational Vortex. Aero. Rept. LR-378, National Research Council, Canada.

Gore, R. W. and Ranz, W. E. (1964): Backflows in Rotating Fluids Moving Axially Through Expanding Cross-Sections. Am. Inst. Chem. Eng. J., 10, pp. 83-88.

Hall, M. G. (1961): A Theory for the Core of a Leading Edge Vortex. J. Fluid Mech., 11, 2, pp. 209-228.

Hall, M. G. (1965): A Numerical Method for Solving the Equations for a Vortex Core. RAE TR 65106, Royal Aircraft Establ., Farnborough, England.

Hall, M. G. (1966a): The Structure of Concentrated Vortex Cores. Progress in Aeronautical Sciences, D. Küchemann, Ed., Vol. 7, Pergamon Press, Oxford, pp. 53-110.

Hall, M. G. (1966b): On the Occurrence and Identification of Vortex Breakdown. RAE TR 66283, Royal Aircraft Establ., Farnborough, England.

Hall, M. G. (1972): Vortex Breakdown. Annual Review of Fluid Mechanics, Vol. 4, Annual Reviews Inc., Palo Alto, Calif.

Harvey, J. K. (1962): Some Observations of the Vortex Breakdown Phenomenon. J. Fluid Mech., 14, 4, pp. 585-592.

Hummel, D. (1965): Untersuchungen über das Aufplatzen der Wirbel an schlanken Deltaflügeln. Zeitschrift für Flugwissenschaften, 13, 5, pp. 158-168.

Lambourne, N. C. and Bryer, D. W. (1961): The Bursting of Leading-Edge Vortices--Some Observations and Discussion of the Phenomenon. ARC R and M No. 3282, Aeronautical Research Council (Britain).

Lavan, Z. and Fejer, A. A. (1966): Investigation of Swirling Flows in Ducts. Technical Report No. ARL-66-0083, Aerospace Research Laboratories, Wright-Patterson AFB.

Leibovich, S. (1968): Axially-Symmetric Eddies Embedded in a Rotational Stream. J. Fluid Mech. 32, pp. 529-548.

Lewellen, W. S. (1971): A Review of Confined Vortex Flows. NASA CR-1772.

Ludwieg, H. (1962): Zur Erklärung der Instabilität der über angestellten Deltaflügeln auftretenden freien Wirbelkerne. Z. Flugwiss., 10, pp. 242-249.

Ludwieg, H. (1965): Erklärung des Wirbelaufplatzens mit Hilfe der Stabilitäts-theorie für Strömungen mit schraubenförmigen Stromlinien. Z. Flugwiss., 13, pp. 437-442.

Mager, A. (1970): Incompressible, Viscous, Swirling Flow Through a Nozzle. AIAA Paper 70-51, AIAA, New York.

Mager, A. (1971): Incompressible, Viscous, Swirling Flow Through a Nozzle. AIAA Journal, 9, 4, pp. 649-655.

Maxworthy, T. (1967): The Flow Creating a Concentration of Vorticity Over a Stationary Plate. Jet Propulsion Laboratory Space Programs Summary 37-44, 4, 243.

McCormick, B. W., Tangler, J. L., and Sherrieb, H. E. (1968): Structure of Trailing Vortices. J. of Aircraft, 5, 3, pp. 260-267.

Mitra, N. K. (1970): Application of the Method of Weighted Residuals in the Computation of Laminar Compressible Boundary Layers. Ph.D. Thesis, Mechanical Engineering Dept., University of California, Santa Barbara, Calif. (available through University Microfilms, Ann Arbor, Michigan).

Mitra, N. K. and Bossel, H. H. (1971): Compressible Boundary Layer Computation by the Method of Weighted Residuals Using Exponentials. AIAA Journal, 9, 12, pp. 2370-2377.

Nissan, A. M. and Bresan, V. P. (1961): Swirling Flow in Cylinders. Am. Inst. Chem. Eng. J., 7, pp. 543-547.

Orloff, K. L. (1971): Experimental Investigation of Upstream Influence in a Rotating Flowfield. Ph.D. Thesis, Mechanical Engineering Dept., University of California, Santa Barbara Calif. (available through University Microfilms, Ann Arbor, Michigan).

Orloff, K. L. and Bossel, H. H. (1971): Laser-Doppler Velocity Measurements of Swirling Flows with Upstream Influence. Bull. Amer. Phys. Soc. (2) 16, pp. 1331 (abstract only).

Potter, A. E., Jr.; Wong, E. L.; and Berlad, A. L. (1958): Stability of Propane-Air Flames in Vortex Flow. NACA TN 4210.

Rosenzweig, M. L.; Ross, D. H.; and Lewellen, W. S. (1962): On Secondary Flows in Jet-Driven Vortex Tubes. J. Aerospace Science, 29, 1142.

Sarpkaya, T. (1971a): On Stationary and Traveling Vortex Breakdowns. J. Fluid Mech., 45, 3, pp. 545-559.

Sarpkaya, T. (1971b): Vortex Breakdown in Swirling Conical Flows. AIAA Journal, 9, 9, pp. 1792-1799.

So, K. L. (1967): Vortex Phenomena in a Conical Diffuser. AIAA Journal, 5, pp. 1072-1078.

Timm, G. K. (1967): Survey of Experimental Velocity Distributions in Vortex Flows with Bibliography. Boeing Scientific Research Laboratories, Document D1-82-0683.

Torrance, K. E. and Kopecky, R. M. (1971): Numerical Study of Axisymmetric Vortex Breakdowns. NASA CR-1865.

Vaisey, G. (1956): 'Reversed Flow' due to Swirl in a Viscous Fluid Moving Along a Tube. 9th Int'l Congress for Applied Mechanics 3, p. 339.

Vogel, H. U. (1968): Experimentelle Ergebnisse über die laminare Strömung in einem zylindrischen Gehäuse mit darin rotierender Scheibe. Bericht 6/1968, Max-Planck-Institut für Strömungsforschung, Göttingen.

Vonnegut, B. (1954): A Vortex Whistle. J. Acoust. Soc. America, 26, p. 18.